



The origin of fluorite deposits in the Bou-Izourane district (Central High Atlas of Morocco) and its relationships with the Tamazeght magmatic complex

Jamal Achmani, Thomas Blaise, Ilham Chraibi, Jocelyn Barbarand, Benjamin Brigaud, Hassan Bounajma

► To cite this version:

Jamal Achmani, Thomas Blaise, Ilham Chraibi, Jocelyn Barbarand, Benjamin Brigaud, et al.. The origin of fluorite deposits in the Bou-Izourane district (Central High Atlas of Morocco) and its relationships with the Tamazeght magmatic complex. *Ore Geology Reviews*, 2023, 160 (105596), pp.105596. 10.1016/j.oregeorev.2023.105596 . hal-04174731

HAL Id: hal-04174731

<https://hal.science/hal-04174731>

Submitted on 4 Aug 2023

HAL is a multi-disciplinary open access archive for the deposit and dissemination of scientific research documents, whether they are published or not. The documents may come from teaching and research institutions in France or abroad, or from public or private research centers.

L'archive ouverte pluridisciplinaire **HAL**, est destinée au dépôt et à la diffusion de documents scientifiques de niveau recherche, publiés ou non, émanant des établissements d'enseignement et de recherche français ou étrangers, des laboratoires publics ou privés.



The origin of fluorite deposits in the Bou-Izourane district (Central High Atlas of Morocco) and its relationships with the Tamazeght magmatic complex

Jamal Achmani ^{a,b,*}, Thomas Blaise ^a, Ilham Chraibi ^b, Jocelyn Barbarand ^a, Benjamin Brigaud ^a, Hassan Bounajma ^c

^a Université Paris-Saclay, CNRS, GEOPS, 91405 Orsay, France

^b Laboratoire de Géosciences, Géo-environnement et Prospection Minière et Hydrique, Département de Géologie, Faculté des Sciences, Université Mohammed Premier, Oujda, Morocco

^c Division exploration minière, Compagnie Minière de Touissit, Morocco

ARTICLE INFO

Keywords:

Moroccan High Atlas
Bou-Izourane deposits
Fluorite mineralization
Tamazeght carbonatite
Fluid inclusions
Late magmatic fluid

ABSTRACT

Fluorite deposits in the Bou-Izourane district of the High Atlas in Morocco are distributed over seven known mineralized sites near the Middle Eocene Tamazeght magmatic complex and hosted in sedimentary rocks (limestones and marls) of the Lower Jurassic (Bou-Izourane, Takkat, Bou-Kharouba and Tabja deposits), magmatic rocks (Bou-Imtessene and Meghsan deposits) and skarns (Tamazeght and Bou-Imtessene deposits). This paper examines the origin of the mineralizing fluids and the relationship between the Tamazeght complex and fluorite deposits. Fluorspar occurs in veins oriented according to three families (N20, N50–80 and N120), in karst cavities and as stratabound deposits. Three stages are identified in the mineralization: (1) fluorite emplacement associated with the dissolution of the host rocks; (2) fracturing and sealing by calcite and finally (3) silicification associated with the partial dissolution of fluorite and calcite. Fluid inclusions in fluorite hosted in marls and carbonates of the Lower Jurassic have low salinities (1.5 to 3 wt% equiv. NaCl) and homogenization temperatures between 91 °C and 159 °C. Fluid inclusions in the Tabja, Tamazeght and Meghsan fluorites exhibit the same salinity range, but with increased homogenization temperatures, ranging from 99 °C to 241 °C, with a vapour phase containing CO₂. Secondary solid daughter phases, such as nahcolite, calcite and strontianite are identified. Only Bou-Imtessene fluorite has high salinity fluid inclusions (~18 wt% equiv. NaCl) and intermediate homogenization temperatures between 126 °C and 187 °C. These high local salinities and the presence of nahcolite and secondary carbonates in the fluid inclusions of the Tabja, Tamazeght and Meghsan fluorites may reflect the involvement of late-magmatic fluids. The δ¹⁸O isotopic composition of the fluid that precipitated calcites from Tabja (highest Th) and Bou-Izourane (lowest Th) indicates a meteoric origin. Fluorite has a broadly similar REE distribution to that of the Tamazeght carbonatites, suggesting that REE are derived from: i) carbonatites by hydrothermal alteration (e.g., Bou-Izourane, Bou-Kharouba and Takkat), and ii) carbonatitic (late-magmatic) fluids (e.g., Tabja, Tamazeght, Meghsan and Bou-Imtessene). Our data shows that fluorite mineralization in the Bou-Izourane district and the spatially associated middle Eocene Tamazeght magmatism have a direct genetic relationship through the contribution of late-magmatic F-rich fluids in close proximity to the complex. Fluorite mineralization farther from the complex is formed by per descensum circulation of meteoric waters along fractures resulting in fluorine leaching. The Tamazeght complex acts as a heat source and driving mechanism for fluid flows. The dissolution and recrystallization reactions are made possible by a strong geothermal gradient persisting after the complex was emplaced. The upwelling of these hydrothermal fluids into the calcium-rich host rocks (limestone and marl) leads to the precipitation of fluorite.

* Corresponding author at: Université Paris-Saclay, CNRS, GEOPS, 91405 Orsay, France.

E-mail address: jamal.achmani@universite-paris-saclay.fr (J. Achmani).

1. Introduction

The Bou-Izourane district, located in the Central High Atlas of Morocco, is one of the top ten fluorite deposits producing in Morocco. GLOBAL MINES has been mining fluorite from the Bou-Izourane deposit since 2004. This company was the first to market this ore for many countries around the world (Italy, France, ...). The annual production capacity of 97% CaF₂ fluorite concentrate reaches 10 kt (Achmani, 2017; Achmani et al., 2020).

Fluorite mineralization in the Bou-Izourane district occurs in the sedimentary cover to the south-east and south-west of the Tamazeght magmatic complex, which is dated as middle Eocene (Tisserant et al., 1976) (Fig. 1). Fluorite mineralization in the Bou-Izourane area and the Tamazeght complex is emplaced in both the Liassic sedimentary formations and the Tamazeght magmatic rocks. The Bou-Izourane district consists of three sites – Bou-Izourane, Bou-Kharouba and Takkat – located in its eastern part. In the three sites, fluorite deposits are hosted by early Jurassic marls and carbonates. The western part of the district

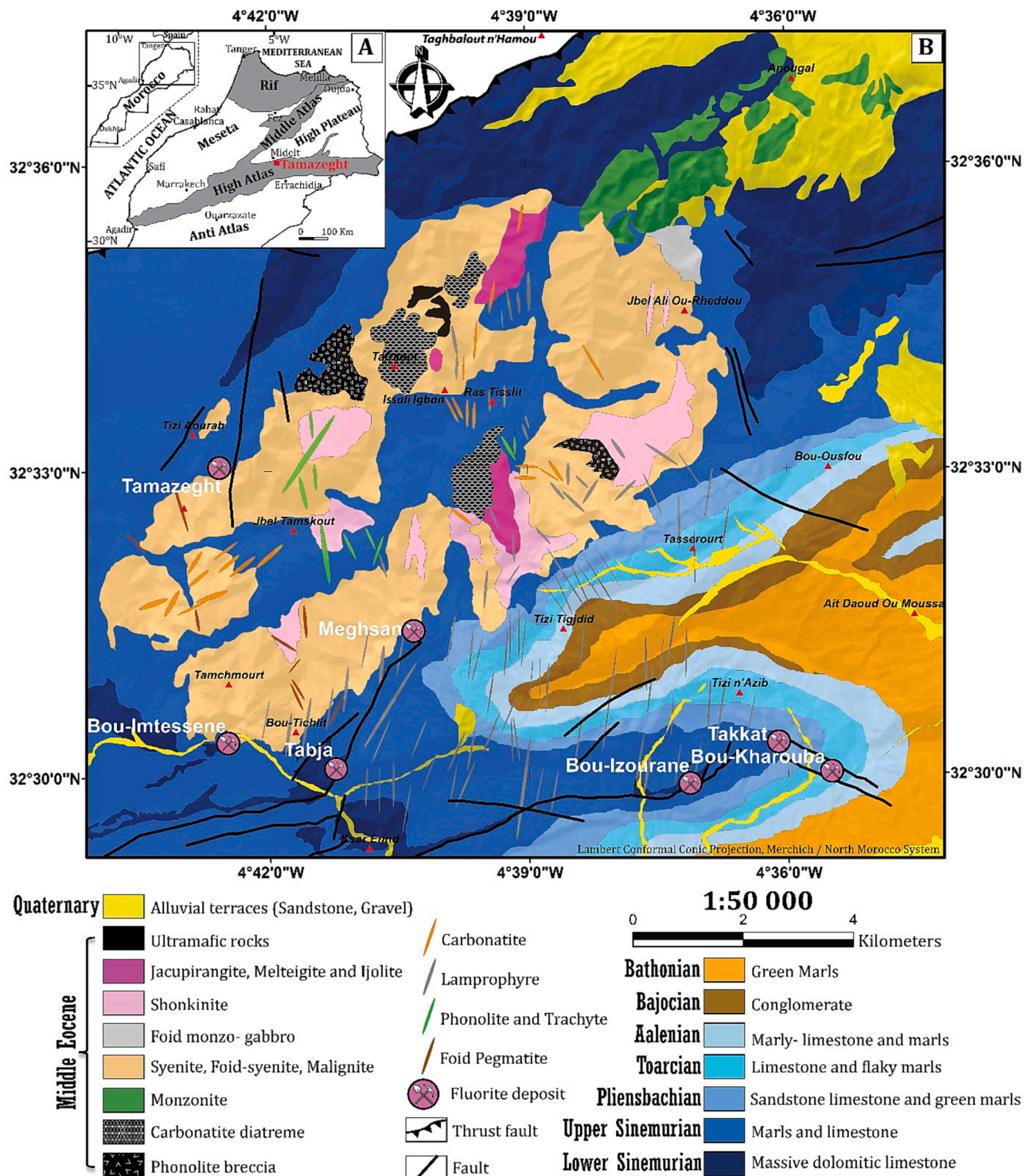


Fig. 1. (A). Simplified structural map of northern Morocco. (B). Geological setting of the study area (Tamazeght complex and Bou-Izourane district) (after Agard, 1973; Kcht, 1990; Marks et al., 2008; Schilling et al., 2009; Bouabdellah et al., 2010b; Achmani, 2017 (modified)).

hosts four other sites (Tabja, Bou-Imtessene, Meghsan and Tamazeght) whose mineralization is hosted either in the Liassic formations, or in the metamorphic aureole of the complex related to the skarns, or finally in the middle Eocene syenites of the Tamazeght magmatic complex (Fig. 1). The sedimentary rocks were strongly deformed during the Atlas orogeny that took place between the end of the Eocene and the Quaternary (Frizon de Lamotte et al., 2000, 2009; Leprêtre et al., 2015).

These mineralizations located in the heart of the High Atlas Range and close to a syenitic-carbonatitic magmatic complex raise the question of their genesis. Two fluorite deposits in Morocco show similarities with the Bou-Izourane mineralization and the Tamazeght complex. The Jbel Tirremi fluorite in the Horst Country Range (eastern Morocco) shows geometric relationships with Eocene-age lamprophyre veins, but fluid analysis has shown no relationship between these magmatic formations and mineralization (Bouabdellah et al., 2014). Conversely, the world-class El Hammam deposit in Central Morocco is characterized by rare earth element enrichment in fluorite, interpreted as evidence of a strong link to Triassic magmatism, where fluorite emplacement is related to the circulation of magmatic fluids from the late- to post-magmatic crystallization of granitic intrusions (Jébrak et al., 1984; Cheillett et al., 2010; Chraibi et al., 2013).

More widely, the existence of fluorite deposits related to carbonatites is proven in several districts (Namibia, Bühn et al., 2002; Russia Redina et al., 2021 or India, Singh et al., 2022), with syenites (Turkey, Coşanay et al., 2017) or with skarns (Mongolia, Duan et al., 2020; Mexico, Camprubí et al., 2019). Other stratiform and/or stratabound-type deposits, unrelated to magmatism, have been described, for example on the periphery of the French Massif Central (Chaillac deposit, Sizaret et al., 2009; Pierre Perthuis stratabound fluorite deposits, Gigoux et al., 2015, 2016; Lenoir et al., 2021).

The genetic link between magmatism and fluorite mineralization can therefore be variable. Fluorite may derive from magmatic to late-magmatic fluids (i.e., felsic magmas; Schönenberger et al., 2008; Cheillett et al., 2010; Bouabdellah et al., 2010a), or formed from hydrothermal fluids of variable origins without a direct connection to magmatic fluids (i.e., Mississippi Valley Type (MVT) deposits; Jemmali et al., 2017; Bouabdellah et al., 2014; Sánchez et al., 2009; González-Partida et al., 2003). Magmatic rock intrusions can, however, play an indirect role, providing a heat source and fluorine- and calcium-rich minerals that can be partially dissolved and recrystallized (Rajabzadeh, 2007; Boiron et al., 2002, 2010; Pei et al., 2017; Ye and Bai, 2022). Preliminary studies by Sośnicka et al. (2021) show that the fluorites from the Bou-Izourane district may have a varied origin. These authors document high salinities (21.2 NaCl wt.% equiv.) in fluid inclusions trapped in fluorite emplaced in close proximity to syenites of the Tamazeght complex. These fluids are interpreted as late-magmatic. Much lower salinities (1.6–8.5 wt% NaCl equiv.) have been documented in fluid inclusions trapped in carbonate-hosted fluorites.

The objective of this paper is to propose a metallogenetic model of fluorite genesis in the Bou-Izourane district and the Tamazeght complex. Particular attention is paid to the origin of the mineralizing fluids and the relationship between the Tamazeght magmatic complex and the mineralizations. To this end, we complement the preliminary results of Sośnicka et al. (2021) with petrographic observations, microthermometric and Raman spectroscopy data of fluid inclusions, and geochemical analyses of trace elements (fluorite and calcite) and stable isotope compositions (O and C) of fluorite-associated calcites. This model will help guide the exploration and mining strategy for fluorite in the district.

2. Geological setting of the deposits

2.1. Regional geology

The Bou-Izourane region is located in the eastern part of the Central High Atlas and is formed by folded Lower to Middle Jurassic terrains (Sinemurian to Bathonian stages) with lithologies which are generally

marly and carbonate. These sedimentary rocks rest unconformably on Triassic basalts (Heitzmann, 1987), according to a tilted block geometry, acquired during Triassic-Jurassic rifting and which may have followed the structures inherited during the Paleozoic Variscan orogeny (Alvaro et al., 2008; Beauchamp et al. 1996; Burkhard et al. 2006; Choubert and Faure-Muret 1962; Ennih and Liegeois 2001; Frizon de Lamotte et al. 2009; Gasquet et al., 2008; Klitgord and Schouten 1986; Mattauer et al. 1977; Piqué and Michard 1989; Thomas et al. 2002). The entire sedimentary series is intruded by rocks of the middle Eocene Tamazeght magmatic complex (Tisserant et al., 1976). The emplacement of the Tamazeght complex generates the development of skarns within the enclosing rocks, over a distance of about 100 m (Salvi et al., 2000; Kchit, 2007; Achmani, 2017).

The Mesozoic sedimentary series of the Atlas domain begins with detrital and then evaporitic continental deposits of the Upper Triassic. The Triassic period corresponds to an important crustal distension linked to the first stages of rifting, allowing the outpouring of tholeitic basalt flows that top the upper silty evaporitic levels (Laville, 1985; Laville and Piqué, 1992). The Triassic structures are guided by normal faulting of the Variscan structures N50 to N90 and N130 to N160 (Mattauer et al., 1977; Laville et al., 1977; Laville, 1977, 1978; Laville and Piqué, 1991, 1992; Aït Brahim et al., 2002), inducing a general NNW-SSE to NW-SE extension. Intrabasin faults oriented NNE-SSW to NE-SW, are considered as dip-slip extension faults (Mattauer et al., 1977; Laville and Petit, 1984; Beauchamp, 1988).

In the Jurassic, the continental input continued. Following the sea level rise, the Atlantic invaded the basin. Reef structures (Patch Reef) then developed on the rift flanks (Du Dresnay, 1971; Aït Addi and Chafiki, 2013). The Atlas rift aborts during the Lower Liassic (Laville, 1985; Laville and Piqué, 1992; Le Roy et al., 1997). Extensional deformation is now concentrated in the Atlas domain, allowing the development of the subsiding intra-continental basins of the High Atlas and of the Middle Atlas (Choubert and Faure-Muret, 1962), with carbonate platform installation (Laville, 1985). Subsidence of the Atlas basins during the Upper Liassic was controlled by NE normal faults developed in the Lower Liassic (Aït Brahim et al., 2002) and E-W Hercynian crustal fractures reactivated as sub-vertical compressive senestrial rifts (Mattauer et al., 1977). The paleo stress field indicates a NW-SE extension that allows the individualization of a mosaic of broad rhombic depocenters bordered by narrow ripples (Du Dresnay, 1975; Mattauer et al., 1977; Studer and Du Dresnay, 1980; Laville, 1981).

In the Upper Jurassic, the E-W and ENE- WSW direction of sinister strike-slip movement is transformed into reverse fault movement in response to the rotation of the regional stress field. The Jurassic basins of the High Central Atlas and Middle Atlas close (Fedan et al., 1989; Laville and Fedan, 1989). This closure, which began in the Bathonian, propagates from SW to NE during the Upper Jurassic, expressing the first phase of inversion with the emersion of the Atlas domain (Laville and Piqué, 1992). From the Upper Cretaceous to the Paleocene, the stress field shows a compressional direction varying from E-W to ESE-WNW, which is in agreement with the relative dexterous lateral movement of Africa-Iberia, relating to the opening of the South Atlantic during the Albian which induced a counter-clockwise rotation of Africa with respect to Eurasia (Tapponnier, 1977). During the Eocene, the N-S compression recorded in Morocco and affecting the whole of the Western Mediterranean (Tapponnier, 1977) is due to the relative displacement between North Africa and Europe (Olivet et al., 1984). The progressive closure of the Tethys (Ricou, 1994) finally led to a continent-continent collision. It is at this time that the Tamazeght complex was established during this N-S compressive phase. This complex consists of plutonic rocks distributed between ultrabasic cumulates (jacupirangites), differentiated terms (syenites, monzonites) and is cut by late and subvertical dykes (carbonatite, lamprophyre and pegmatites) oriented essentially N00 to N45 and NW-SE (Kchit, 2007; Fig. 1). The mode of emplacement is thought to be related to sinister shearing leading to the migration of magmatic bodies (Kchit, 2007).

The formation history of the Moroccan High Atlas Range begun in the upper Eocene with an early event showing an abrupt transition from marine to a continental conglomerate formation, followed by a quiescence phase related to the relaxation of horizontal orogenic stresses at the African/European plate boundary, in the Oligocene and Lower Miocene. The Lower-Middle Miocene period is characterized by a first phase of lithospheric thinning plus a shortening component which triggered the emplacement of tectono-gravity sheets along the High Atlas, and this was followed by a large-scale subsidence state related to a decrease in the intensity of lithospheric thinning. During the Pliocene-Quaternary, shortening resumed and led to the construction of the present orogen with a contribution from a second lithospheric thinning event (Frizon de Lamotte et al., 2000, 2009; Leprêtre et al. 2015).

2.2. Deposit geology

Fluorite occurs in veins oriented in three families: N20, N50-80 and N120, as well as in karst cavities and along strata-bound joints between marl and limestone (Table 1; Fig. 2). The extension of the vein mineralization varies from 20 to 500 m with a strength of up to 5 m. The volumes of mineralization hosted in the karst cavities vary between 10 and 4000 m³.

2.2.1. Mineralization hosted in the sedimentary cover

Fluorite mineralization at the Bou-Izourane, Takkat, Bou-Kharouba and Tabja sites is hosted in marl and carbonate rocks of the sedimentary cover. The mineralization mined at the Bou-Izourane site is mainly stratiform, with mineralized fractures oriented N20, N50-80, N120, and fills karstic cavities (Table 1; Fig. 2A, E and Appendix A (Fig. A.1A)), of light purple brecciated fluorite and is cut by calcite veinlets (Fig. 2B, F and Table S1 (Appendix B)). The Takkat fluorite is light purple, fractured, and veinlet-like in massive dolomitic limestones of Lower Sinemurian age overlain by marl-layered bedded limestones of Upper Sinemurian age (Table S1 (Appendix B)). Two sites are mined: i) to the south, within veins oriented N120; ii) to the north, within veins oriented N20 (Table 1; Appendix A (Fig. A.1B)). At Bou-Kharouba, fluorite is colourless to light purple within N120-trending veins averaging 2 m in thickness, cutting Toarcian marl and limestone beds (Table 1; Appendix A (Fig. A.1C) and Table S1 (Appendix B)). At the Tabja site, fluorite is hosted in massive dolomitic limestones in two forms (Table 1): i) vein-like, in which purple fluorite and white calcite with a greenish tendency are found (Appendix A (Fig. A.1D)); ii) within karst cavities (Fig. 2G), where purple fluorite with light grey-green patches, representing silification of fluorite, is found (Fig. 2H).

2.2.2. Mineralization hosted in the skarns

The Tamazeght and some of the Bou-Imetssene deposits are hosted in skarns (Table 1). The Tamazeght site is also characterized by well-

crystallized lilac-purple fluorite in cavities developed in the skarns (Appendix A (Fig. A.2A) and Table S1 (Appendix B)). As for Bou-Imetssene, skarn-hosted fluorite appears as purple spots disseminated in the skarns (Appendix A (Fig. A.2B) and Table S1 (Appendix B)).

2.2.3. Mineralization hosted in the syenites

At Bou-Imetssene, other fluorite mineralization occurs as lilac-hued fluorite stock-works, oriented N50-80 and N120, intersecting the Tamazeght syenites (Table 1; Fig. 2C, D and Appendix A (Fig. A.3B)). Fluorite at the Meghsan site occurs as dark purple cubes (antozonite-type fluorite) (Appendix A (Fig. A.3A) and Table S1 (Appendix B)), this vein mineralization oriented N50-80, intersects both the Liassic formations and the Tamazeght skarns and syenites.

3. Materials and methods

Seven fluorite mineralized sites (Bou-Izourane, Bou-Kharouba, Takkat, Tabja, Meghsan, Tamazeght and Bou-Imetssene) were studied (Fig. 1). After sampling (Table S1 (Appendix B)), petrographic observations were made by optical microscopy, cathodoluminescence (CL) microscopy, and scanning electron microscopy (SEM) on thin sections and on fragments mounted in epoxy and then polished, at the Geosciences Paris-Saclay (GEOPS) laboratory. CL observations were performed on an Olympus BX41 microscope coupled to a Cathodyne cold cathode cathodoluminescence (NewTec) operating at 10–12 kV and 160–260 μA and a Qicam Fast 1394 digital camera. SEM images were produced at an accelerating voltage of 15 keV and semi-quantitative elemental compositions were measured by energy dispersive spectrometry (EDS) at an accelerating voltage of 15 keV and an accumulation time of 30 s.

14 fluorite samples from different sites in the Bou-Izourane district and the Tamazeght complex were selected for microthermometric analysis of fluid inclusions. Homogenization (Th) and water ice melting temperatures (Tm) of the two-phase aqueous inclusions were acquired using a LINKAM MDS600 cooling and heating stage, mounted on a Leica microscope and equipped with a Lumenera Infinity 3 camera, at GEOPS. Each fluid inclusion was measured twice. Data that cannot be replicated was excluded. The few fluid inclusions belonging to the same plane having variable liquid-vapour ratios were excluded and considered as evidence of post-trapping deformation (stretching, leakage) or necking-down (Goldstein and Reynolds, 1994). The uncertainties associated with Th and Tm measurements are ± 1.0 °C and ± 0.1 °C, respectively. The solid phases contained in some of the fluid inclusions were identified by Raman spectroscopy (LabRAM (Horiba) at the GeoRessources laboratory of the University of Lorraine) with a 300 mW 514.71 nm green laser (Cobolt Fandango 300), an 1800 rpm grating and a x100 objective. The confocal hole was open at 700 μm and the slit at 200 μm. The acquisition is done in the range of 950 to 1075 cm⁻¹ for solids and 1400 to 3500

Table 1

Geometric characteristics of the mineralization in different sites of the Bou-Izourane district and Tamazeght complex.

Mineralized site	Host rock	Type of mineralization	Direction	Extension	Thickness/Dimensions
Bou-Izourane	Limestone to marls (Lower Jurassic)	Veins	N20	70 to 200 m	1 to 5 m
			N50-80	20 to 500 m	2 to 5 m
		Karstic cavities	—	—	1000 to 4000 m ³
Bou-Kharouba	Limestone to marls (Lower Jurassic)	Strata-bound joints	—	30 to 100 m	0.2 to 1 m
	Limestone to marls (Lower Jurassic)	Veins	N120	40 to 70 m	0.5 to 2 m
Takkat	Limestone to marls (Lower Jurassic)	Veins	N20	100 to 500 m	0.5 to 4 m
			N120	20 to 60 m	1 to 2 m
Tabja	Limestone to marls (Lower Jurassic)	Veins	N20	20 to 110 m	0.5 to 3 m
			N50-80	30 to 170 m	1 to 3 m
Tamazeght	Skarns	Karstic cavities	—	—	10 to 30 m ³
		Karstic cavities	—	—	30 to 70 m ³
		Veins	N50-80	60 to 200 m	0.5 to 2 m
Meghsan	Syenites	Stockwork	N120	170 to 300 m	1 to 2 m
Bou-Imetssene	Syenites	Stockwork	N50-80	50 to 110 m	0.5 to 2 m
	Skarns				

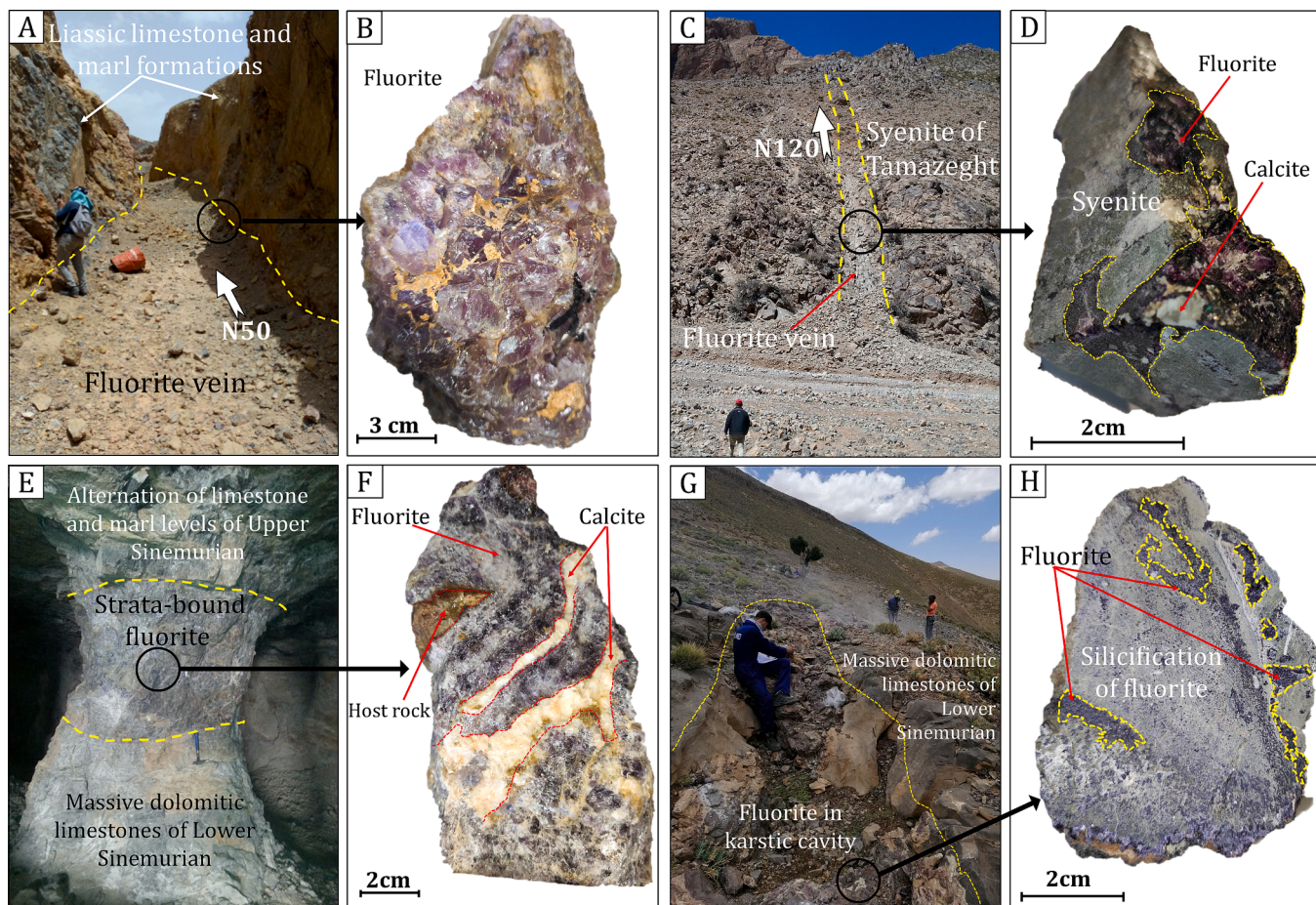


Fig. 2. Photographs illustrating the types of fluorite mineralization in the Bou-Izourane district. (A, B). Fluorite vein intersecting the Liassic marly limestone formations in the central site of Bou-Izourane with a hand specimen of fluorite. (C, D). Fluorite vein intersecting the Eocene syenites of Tamazeght in the Bou-Imtessene site with a specimen of fluorite. (E, F). Fluorite occupies the strata joints between massive dolomitic limestones and marl-limestones in the Bou-Izourane site with a specimen of fluorite. (G). Fluorite in karstic cavity in massive dolomitic limestone at the site of Tabja. (H). fluorite specimen from the Tabja site with silicification patches replacing fluorite.

cm^{-1} for OH. The acquisition time and the number of accumulations are fixed in order to optimize the signal/background ratio.

Minor and trace elements in calcite and fluorite were measured using a Thermo Scientific™ Element XR ICP-MS coupled to a Teledyne Photon Machines 193 nm ArF laser ablation (LA) system, at GEOPS ([Appendix A](#) ([Fig. A.7](#))). Fluorite crystals were ablated at a fluence of 6.25 J.cm^{-2} , with an ablation diameter of $85 \mu\text{m}$ and a pre-ablation diameter of $110 \mu\text{m}$. The conditions for calcite analysis are a fluence of 2 J.cm^{-2} with an ablation diameter of $150 \mu\text{m}$ and a pre-ablation of $155 \mu\text{m}$. Each fluorite and calcite sample was ablated at a frequency of 10 Hz with a 30 s background acquisition followed by 30 s of ablation. Elemental concentrations of calcites were calibrated using NIST612 glass reference material, and the carbonate pellet MACS-3 (United States Geological Survey (USGS)) was used as secondary reference material to ensure accuracy. In the absence of fluorite reference material, we used an in-house fluorite sample Pierre-Perthus 16 (PP16) for quality control, sample consisting of yellow fluorite crystals which was analyzed by ICP-MS after dissolution ([Gigoux et al., 2015; Gigoux, 2015](#)). The 59 measurements performed on the NIST 612 glass reference material ([Pearce et al., 1997](#)) during this study gives an accuracy ranging from 1.4% to 7.6% on elemental concentrations. ^{43}Ca was used as internal standard to convert intensities into concentrations. For fluorite analysis, we used a CaO value set at 71.83 wt% oxide (wt % CaO), corresponding to the value of stoichiometric fluorite. Similarly, a CaO value set at 56.03 wt% was used for calcite. Data was reduced using Iolite 4 software ([Paton et al., 2011](#)). The precision and accuracy of the elemental concentrations

measured in fluorite and calcite was evaluated using the matrix-match reference materials MACS-3 (calcite) and PP16 (fluorite). The results of Rare Earth Element (REE) quantifications in MACS-3 carbonate reference material and in-house fluorite material “PP16” are listed in [Table S5, S6 \(Appendix B\)](#). The distributions obtained on “PP16” by LA-ICP-MS are compared to the distribution obtained by dissolution - ICP-MS ([Gigoux, 2015](#)) in [Fig. A.6A \(Appendix A\)](#), and similarly, the values obtained on MACS-3 are compared to their certified values (USGS, Tb and Yb values are from [Jochum et al., 2012](#)) in [Fig. A.6B \(Appendix A\)](#). The distribution of REE for fluorite samples by dissolution - ICP-MS for the different sites of the Bou-Izourane district and the Tamazeght complex was published by [Achmani et al., 2020](#). In addition, REE in the host rocks were determined from samples of lamprophyre, carbonatite and syenite, skarns, limestones and marls of the Liassic by dissolution-ICP-MS (ALS Ireland, Geochemistry method ME-MS81 and Bureau Veritas Minerals Canada, Exploration Geochemistry, method MA250) ([Table S4 \(Appendix B\)](#)). Before dissolution, the samples were washed and rinsed with distilled water and then crushed. These analyses are complemented in this paper by data from the works of [Bouabdelli et al., 1988](#) (lamprophyre); [Kchit, 2007](#) and [Bouabdellah et al., 2010b](#) (carbonatite) and [Wang et al., 2016](#) (syenite).

Two hydrothermal calcite filling fractures in the Tabja and Bou-Izourane deposits were sampled to measure their O and C stable isotopic composition ([Appendix A](#) ([Fig. A.7A, D](#))). After acid digestion of calcite powders, CO_2 was analyzed using a dual-inlet Isoprime 100 spectrometer (Elementar) coupled to a multi-Carb system at the

Laboratory of Sciences of Climate and Environment (LSCE; Paris-Saclay University). Data was standardized to Pee Dee Belemnite (PDB) based on repeated measurements of international reference materials NBS19 and NBS18. The 1SD external reproducibility of the in-house laboratory carbonate standard (MARGO) is 0.05 ‰ for $\delta^{18}\text{O}$ and 0.03 ‰ for $\delta^{13}\text{C}$. A sufficient amount of calcite powder was extracted from each sample to perform two measurements. The difference in the values between the two measurements is less than 0.1 ‰ for both $\delta^{18}\text{O}$ and $\delta^{13}\text{C}$. As a result, the mean value of the two measurements was considered. The fractionation equation of Zheng (1999) was used to recalculate the O isotopic composition of parental fluids.

4. Results

4.1. Petrographic features of fluorite deposits

4.1.1. Bou-Izourane, Bou-Kharouba, Takkat and Tabja fluorite sites:

Mineralization hosted in the sedimentary cover

Bou-Izourane fluorite occurs as a massive, euhedral form (>500 µm) and is light purple in transmitted light (Fig. 3B, C). In cathodoluminescence, the fluorite is blue in colour, with undissolved fragments of calcite from the host oolitic limestone packed within the fluorite (Fig. 3A, D; Appendix A (Fig. A.4A and B)). It is cut by fractures filled with orange coloured calcite in CL (Fig. 3A, C). The automorphic quartz crystals found in the oolitic limestone, are also included in fluorite after dissolution of calcite from the host (Appendix A (Fig. A.4A, B)).

At Takkat, optical and cathodoluminescence microscopy shows euhedral fluorite crystals associated with calcite and micro-quartz (Fig. 3E, G). In cathodoluminescence, calcite precipitated in fractures intersecting the fluorite appears as a homogeneous orange colour and/or a succession of dark orange and luminescent zones (Fig. 3F). Micro-metric quartz comes later and replaces the fluorite and calcite (Appendix A (Fig. A.4C)). Fragments of the country rock remained included in the fluorite (Appendix A (Fig. A.4C)).

The fluorite from Bou-Kharouba has the same petrographic characteristics as the fluorite from Bou-Izourane and Takkat (Fig. 3H-J).

At the Tabja site, the fluorite appears under the microscope in massive form and is partially replaced by calcite, which appears to be homogeneous orange in cathodoluminescence (Fig. 4A-C and 5B). In karst cavities, fluorite appears as zoned euhedral crystals (succession of dark blue and blue luminescent bands) in natural light (Fig. 4D, E); blue fluorite in CL is partially replaced by black micro-quartz (Fig. 4F, 5A).

4.1.2. Tamazeght fluorite site: Mineralization hosted in the skarns

Microscopic characterization of the Tamazeght fluorite shows that the emplacement of this fluorite is synchronous with the dissolution of the calcite of the surrounding rock. Micro-quartz precipitates later and replaces the fluorite (Fig. 4G-I). In cathodoluminescence, the euhedral fluorite shows a blue core (Fl1) that wraps around undissolved pieces of orange calcite that belong to the host rock, which is surrounded by the homogeneous blue fluorite (Fl2) (Fig. 4I).

At Bou-Imetssene, the purple fluorite disseminated in the skarns appears as small patches developed on the constituent minerals of the

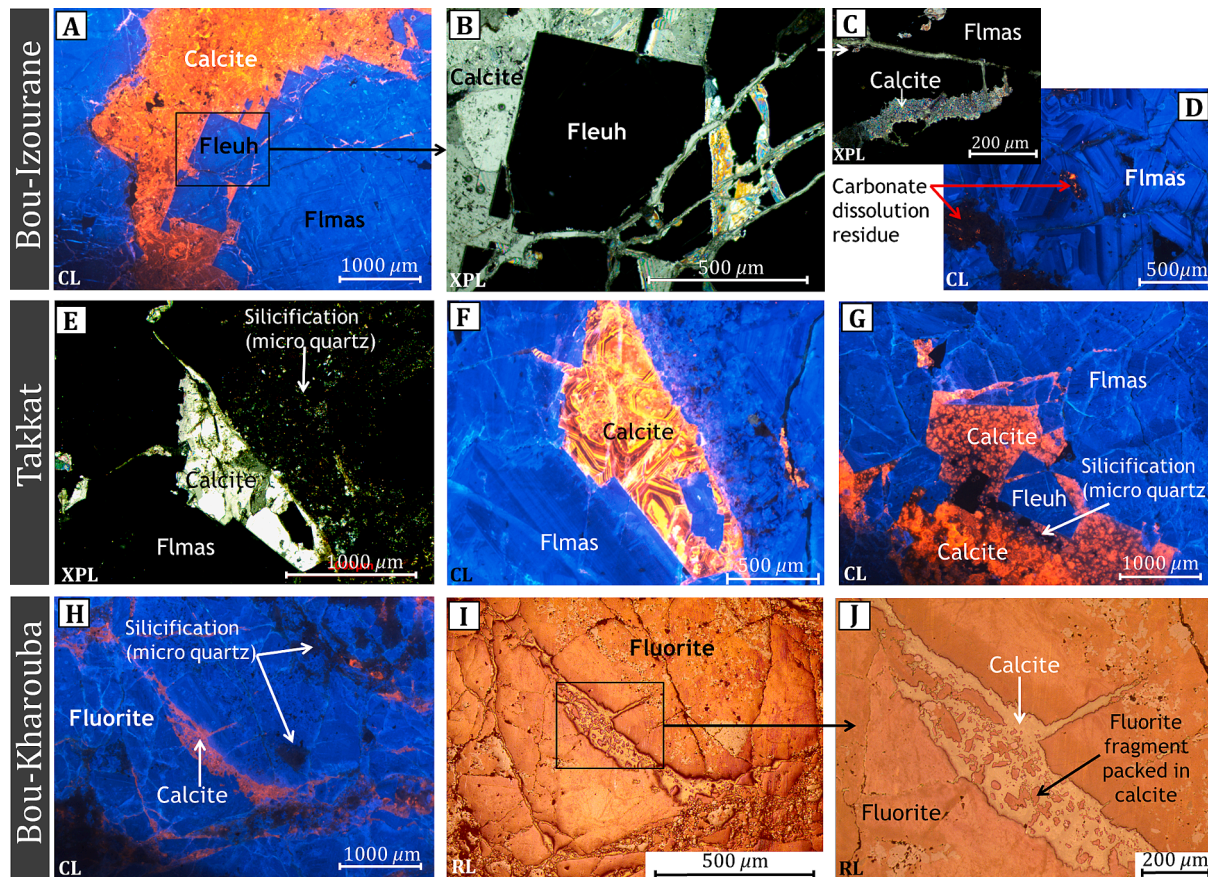


Fig. 3. (A, D). Cathodoluminescence (CL) images of the paragenesis of fluorite mineralization at the Bou-Izourane site. (B). Cross polarized light photography of fluorite from the Bou-Izourane site. (C). Cross polarized light photography of calcite in fractures intersecting fluorite at the Bou-Izourane site. (E). Polarized light photography of quartz replacing fluorite and calcite in the Takkat site (F, G). Cathodoluminescence images of zoned and homogeneous calcite precipitated in the fluorite fractures at Takkat. (H, I and J). Cathodoluminescence image and reflected light images of fluorite-calcite-quartz samples from the Bou-Kharouba site. (Flmas. massive fluorite, Fleuh. euhedral fluorite).

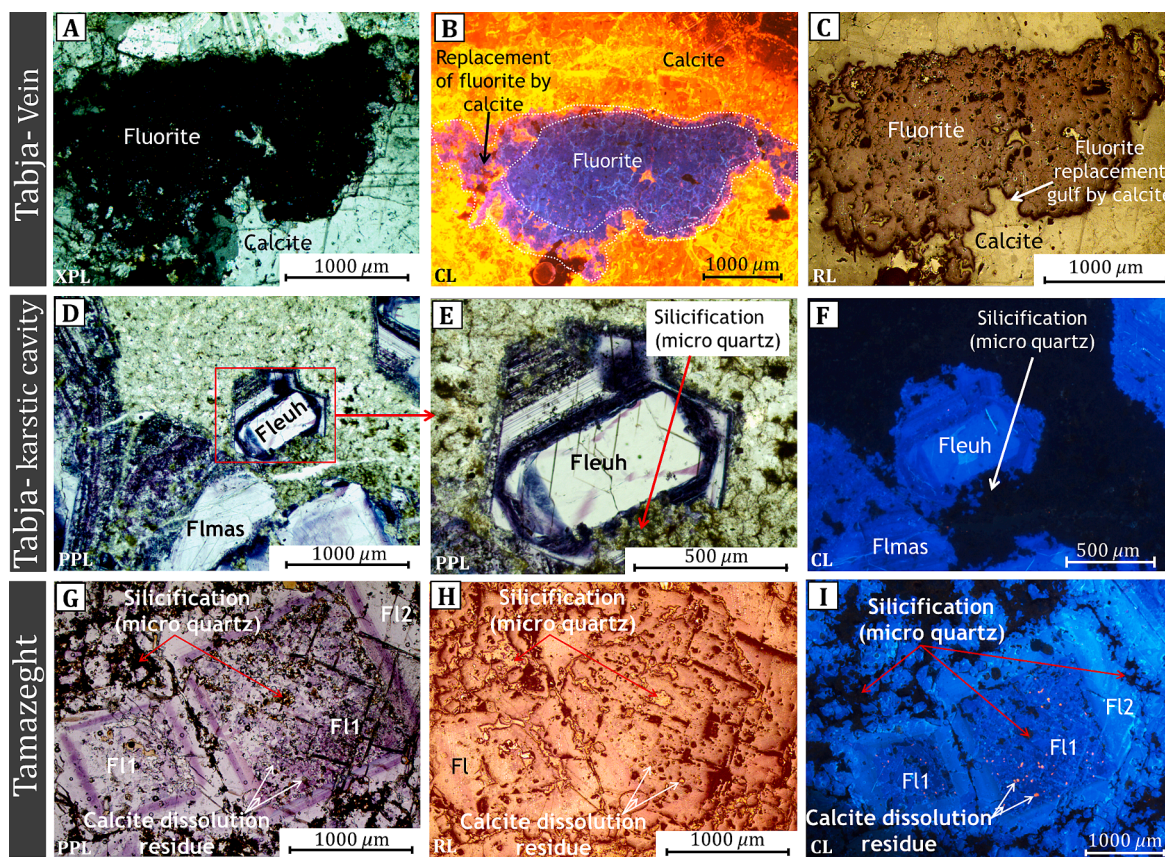


Fig. 4. (A, B, C). Cross polarized light, cathodoluminescence image and reflected light photographs of calcite replacing fluorite from the Tabja vein. (D, E). Plane polarized light photographs of massive and euhedral fluorite with the succession of deep blue and blue luminescent bands blue from the karst cavity of Tabja. (F). Cathodoluminescence image of the quartz (black) replacing the euhedral fluorite crystal in blue from the karst cavity of Tabja. (G, H). Plane polarized and reflected light photographs of zoned purple fluorite with quartz altering Tamazeght fluorite. (I). Cathodoluminescence image of the Tamazeght euhedral fluorite showing a blue core packed with orange calcite residues (Fl1) surrounded by homogeneous blue fluorite (Fl2). (Flmas: massive fluorite, Fleuh: euhedral fluorite).

skarns. In cathodoluminescence, the fluorite appears dark blue and is intersected by fractures filled with orange calcite (Appendix A (Fig. A.2B)). Fragments of undissolved skarn minerals remain included in the fluorite (Appendix A (Fig. A.2B)).

4.1.3. Bou-Imetssene and Meghsan fluorite sites: Mineralization hosted in the syenites

Some of the constituent minerals of the syenites at the Bou-Imetssene site, notably aegirine and potassium feldspar, are replaced by fluorite (Fig. 6A-C). Fluorite occurs in an interstitial form between the minerals forming the syenitic domes of Tamazeght (Appendix A (Fig. A.3B)). Radiation halos are developed in fluorite, around widely dissolved zircons and “uranopyrochlore”-type oxides (Fig. 5E, F). In cathodoluminescence, orange calcite seals fractures that intersect the blue fluorite (Fig. 6A).

The fluorite at the Meghsan site has similar petrographic characteristics to the fluorite hosted in the syenites at the Bou-Imetssene site (Fig. 6D-F and 5C). In cathodoluminescence, the fluorite shows a blue core (Fl1) that contains undissolved orange calcite inclusions from the surrounding rock, and is surrounded by homogeneous blue fluorite (Fl2) (Fig. 6E). Calcite then develops in fractures intersecting the fluorite (Fig. 6D). There is no development of radiation halos despite the presence of undissolved zircon crystals (Fig. 5D). Iron oxides fill cracks intersecting fluorite and calcite (Fig. 6D).

4.2. Fluid inclusions

4.2.1. Fluid inclusion petrography and microthermometry

Primary and secondary inclusions were identified based on inclusion morphology, position relative to growth planes, and phase properties

observed at room temperature (Roedder, 1979, 1984; Van den Kerkhof, 1988; Van den Kerkhof and Hein, 2001; Fig. 7).

The bulk of the observed and analysed fluid inclusions in fluorite crystals correspond to two-phase (liquid + vapor) inclusions with sizes of 3–80 µm, liquid phase dominant (Fig. 7A, B), homogenizing in the liquid phase. These inclusions are interpreted as primary. Secondary inclusions were recognized at the Tabja and Meghsan sites in fluorite crystals. Only fluid inclusions at sites in direct spatial relationship with syenites, notably the Meghsan site, are multiphase, containing liquid, vapour and one or more solids (Fig. 7E). Aqueous two-phase fluid inclusions in calcite, interpreted as primary, have been studied at the Bou-Izourane and Tabja sites (Fig. 7G, H).

Upon cooling of inclusions in fluorite, freezing is observed between -63°C and -36°C . Water ice is the only solid observed at low temperatures and the first melting of this water ice occurs between -30°C and -5°C . Homogenization (Th) and freezing (Tf) temperatures, as well as temperatures of first ice melting (Te) and final ice melting (Tm) measured on primary and secondary two-phase inclusions trapped in fluorite and calcite crystals from different sites in the Bou-Izourane region and the Tamazeght complex, are presented in Table 2. Salinities are calculated from Steele-MacInnis et al. (2012) in the $\text{H}_2\text{O}-\text{NaCl}$ system.

For fluorite crystals, homogenization temperatures of primary fluid inclusions from the Bou-Izourane site show a unimodal distribution, with temperatures ranging from 91°C to 159°C and a mean homogenization temperature value of $123 \pm 15^{\circ}\text{C}$ ($n = 23$) (Fig. 8A). Salinities vary between 0.8 and 3.5 wt% equiv. NaCl. The calcite at Bou-Izourane shows fluid inclusions with homogenization temperatures ranging from 107 to 119°C with an average value of $113 \pm 4^{\circ}\text{C}$ ($n = 10$) as a unimodal distribution (Fig. 8A). At Bou-Kharouba, homogenization

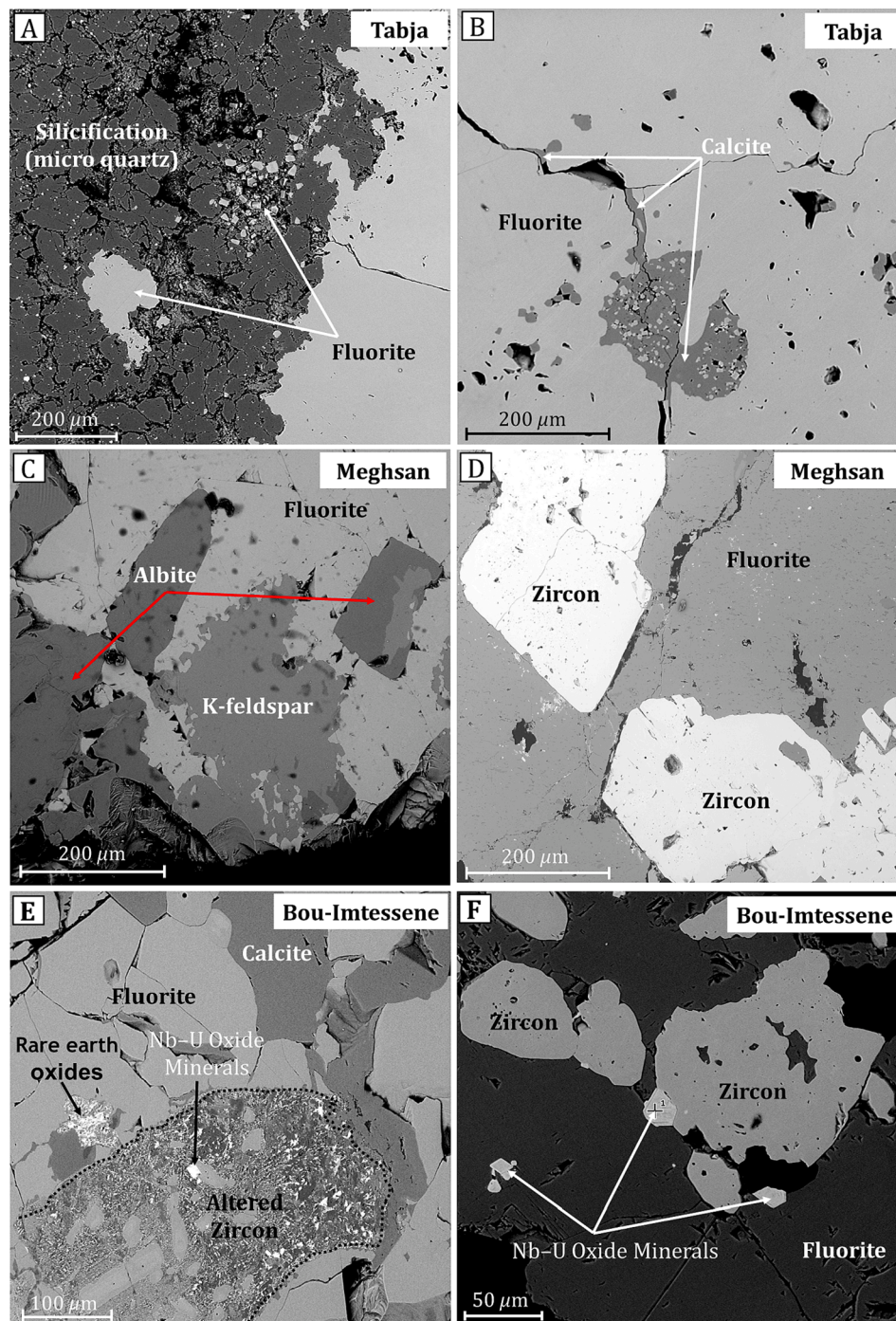


Fig. 5. Scanning electron microscope (SEM) photomicrographs of various petrographic properties of fluorite from Bou-Izourane and Tamazeght complex deposits. (A). Silicification (micro quartz) replacing the fluorite in the Tabja site. (B). Fluorite replaced by calcite in the Tabja site. (C). Syenite minerals replaced by fluorite at the Meghsan site. (D). Undissolved zircons packed in Meghsan fluorite. (E, F). Dissolution of zircons from Bou-Imtessene syenites and rare earths and Nb-U oxides within fluorite crystals at the Bou-Imtessene site.

temperatures ranged from 96 to 125 °C with a mean value of 112 ± 7 °C ($n = 14$) (Fig. 8C), salinity being between 0.9 and 2.9 % NaCl equivalent weight. At Takkat, the average homogenization temperature is 126 ± 8 °C ($n = 15$) and the salinity varies between 1.5 and 3.1 wt% NaCl equivalent (Fig. 8B). At Tamazeght, the inclusions are homogenized at temperatures ranging from 115 to 143 °C with an average value of 129 ± 6 °C ($n = 27$) (Fig. 8G) and have a salinity between 0.2 and 2.7 wt% NaCl equivalent.

At the Tabja and Meghsan sites, homogenization temperatures in fluorite are higher (Appendix A (Fig. A.5)). At the Tabja site, the Th of the primary fluid inclusions ($n = 58$) show a bimodal histogram centred at 90–150 °C and 180–200 °C, and the secondary fluid inclusions ($n = 25$) show temperatures centred between 80 and 100 °C and 120–180 °C

(Fig. 8D, E). The average salinity of the primary fluid inclusions in the fluorite is close to 2.4 wt% equiv. NaCl. For Meghsan fluorite, Th ranges from 169 to 241 °C with an average value of 200 ± 21 °C ($n = 26$) (Fig. 8D), and salinities range from 2.1 to 3.7 wt% equiv. NaCl. For the same sample, homogenization of secondary fluid inclusions ($n = 22$) occurs between 101 and 287 °C, following a bimodal distribution centred at 110–120 °C and 270–280 °C (Fig. 8D). The Tabja calcite has primary fluid inclusions with homogenization temperatures varying between 110 and 142 °C in a unimodal distribution (Fig. 8D). At the Bou-Imtessene site, fluid inclusions in fluorite are very rare, and homogenization temperatures are comparable and vary between 127 and 187 °C (Fig. 8H). On the other hand, salinity is much higher than at the other sites and varies between 17.6 and 18.9 wt% equiv. NaCl.

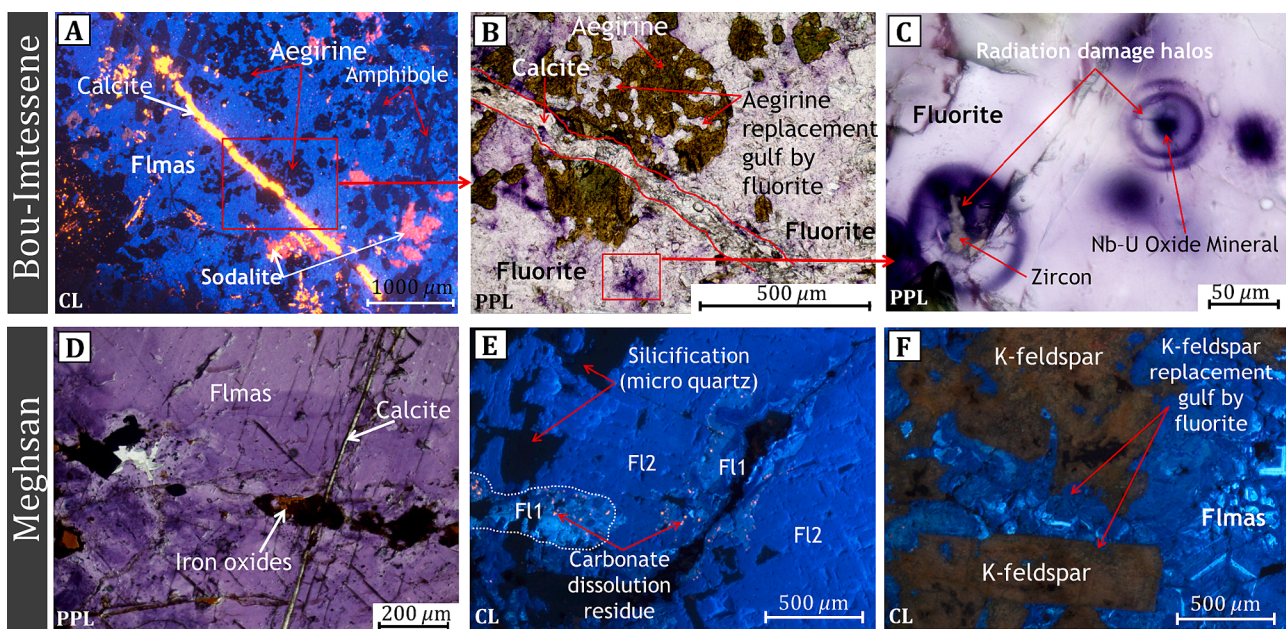


Fig. 6. (A, B). Cathodoluminescence and plane polarized light photographs showing syenite minerals (e.g., Aegirine) replaced by fluorite at the Bou-Imtessene site and calcite later precipitated in the fractures intersecting this fluorite. (C). Irradiation halos the in fluorite of the Bou-Imtessene site. (Fl. Fluorite, Flmas: Massive fluorite). (D). Plane polarized light photograph of the paragenesis of fluorite mineralization at the Meghsan site showing calcite and iron oxides filling fissures intersecting the fluorite. (E). Cathodoluminescence image of the Meghsan fluorite showing a blue core packed with orange calcite residues (Fl1) surrounded by homogeneous blue fluorite (Fl2). (F). Cathodoluminescence image of potassium feldspars in brown replaced by fluorite.

4.2.2. Raman spectroscopy

The solid phases in the inclusions of the Meghsan fluorite crystals have been identified by Raman spectroscopy and correspond to nahcolite (NaHCO_3), strontianite (SrCO_3) and hexahydrite ($\text{MgSO}_4 \cdot 6\text{H}_2\text{O}$). Their frequent presence within the fluid inclusions of a same plane means that they can be identified as secondary solid phases (i.e., precipitated in situ by supersaturation during the cooling of the fluid). The rarest occurrences of barite (BaSO_4) could be interpreted as accidental trapping. Dissolved phosphate is also present in the liquid phase (Fig. 9A, B).

At the Tabja site, calcite and whewellite ($\text{Ca}(\text{C}_2\text{O}_4)_2 \cdot \text{H}_2\text{O}$) are identified as solid phases, with dissolved phosphates and carbonates in the liquid phase. In the Tamazeght site, the fluid inclusions are rich in dissolved CO_2 . Finally, the fluorite crystals at Bou-Imetssene contain solid carbonates, while the liquid phase contains NaCl and dissolved phosphates. For these sites, the origin of the solid phases within the inclusions remains uncertain.

4.3. Carbon and oxygen stable isotope composition

Stable oxygen isotope compositions are similar between calcites from the two sites (Table 3). The $\delta^{18}\text{O}$ value of the Tabja calcite (Fig. 4A-C) is -17.1 ‰ V-PDB . The $\delta^{18}\text{O}$ of the Bou-Izourane calcite (Fig. 3A, B) is -18.7 ‰ V-PDB . The $\delta^{13}\text{C}$ values are also comparable between the two calcites (-0.7 ‰ V-PDB in Tabja calcite and -0.8 ‰ V-PDB in Bou-Izourane calcite).

4.4. Fluorite elemental composition

4.4.1. REE distribution

Detailed results of trace element analyses in fluorite and calcite from each mineralized site are listed in Table S2, S3 (Appendix B). Average trace element concentrations measured in fluorite by LA-ICP-MS are summarized in Table 4. Fluorite hosted in syenites and skarns at the Bou-Imetssene site is enriched in rare earth elements (REE) (ΣREE between 4 ppm and 573 ppm with an average of 61.5 ppm) compared to the other mineralized sites. The REE distributions of this fluorite, normalized to

the chondrites (Sun and McDonough, 1989; Fig. 10A, B), show enrichment in light rare earths (LREE) relative to heavy rare earths (HREE) ($\text{La}_{\text{N}}/\text{Gd}_{\text{N}} = 4.1\text{--}142.4$; $\text{Gd}_{\text{N}}/\text{Yb}_{\text{N}} = 0.8\text{--}9.7$; $\text{La}_{\text{N}}/\text{Yb}_{\text{N}} = 9.2\text{--}357.4$). Calcite shows a similar REE distribution to that of the associated fluorite at the Bou-Imetssene site, with ΣREE ranging from 116 ppm to 206 ppm. Fluorites from the other six sites in the Bou-Izourane district and the Tamazeght complex show that despite their variations in colour and texture, they have comparable, parallel and flat rare-earth distributions (Fig. 10C-H). The sum of the REEs concentrations varies between sites: Bou-Izourane (2–55 ppm), Bou-Kharouba (13–57 ppm), Takkat (3–124 ppm), Tabja (0.6–21 ppm), Meghsan (4–71 ppm) and Tamazeght (8–263 ppm). Rare-earth fractionation in fluorites from these six sites is low ($\text{LREE}_{\text{N}}/\text{HREE}_{\text{N}} = 0.23\text{--}6.53$; $\text{La}_{\text{N}}/\text{Gd}_{\text{N}} = 0.09\text{--}33.94$; $\text{Gd}_{\text{N}}/\text{Yb}_{\text{N}} = 0.15\text{--}3.07$; $\text{La}_{\text{N}}/\text{Yb}_{\text{N}} = 0.13\text{--}27.14$; Fig. 11). The REE distribution of fluorite-associated calcites from these six sites in the Bou-Izourane area and Tamazeght complex (Fig. 10C, D, E, G, H) resemble the REE distributions of fluorites, but are less enriched in heavy REEs (Fig. 10E, G, H).

4.4.2. Other trace elements

Concentrations of other trace elements in the fluorite at the different sites show significant variations, notably in Y (0 to 76 ppm), Sr (38 to 9400 ppm), Mg (40 to 950 ppm), Th (0 to 10 ppm) (Fig. 12). Uranium concentration ranges from 0.1 to 0.7 ppm in the Bou-Imtessene and Tamazeght sites, which are hosted in direct contact with the syenites and skarns (Fig. 12E). Fluorites from the Bou-Imtessene and Meghsan sites have relatively high concentrations of Mg (46 to 950 ppm) and Sr (4900 to 9400 ppm), respectively (Fig. 12A, D).

5. Discussions

5.1. Paragenetic sequence of fluorite mineralization

The general paragenesis of these fluorite mineralizations, whichever site is considered, comprises three stages (Fig. 13).

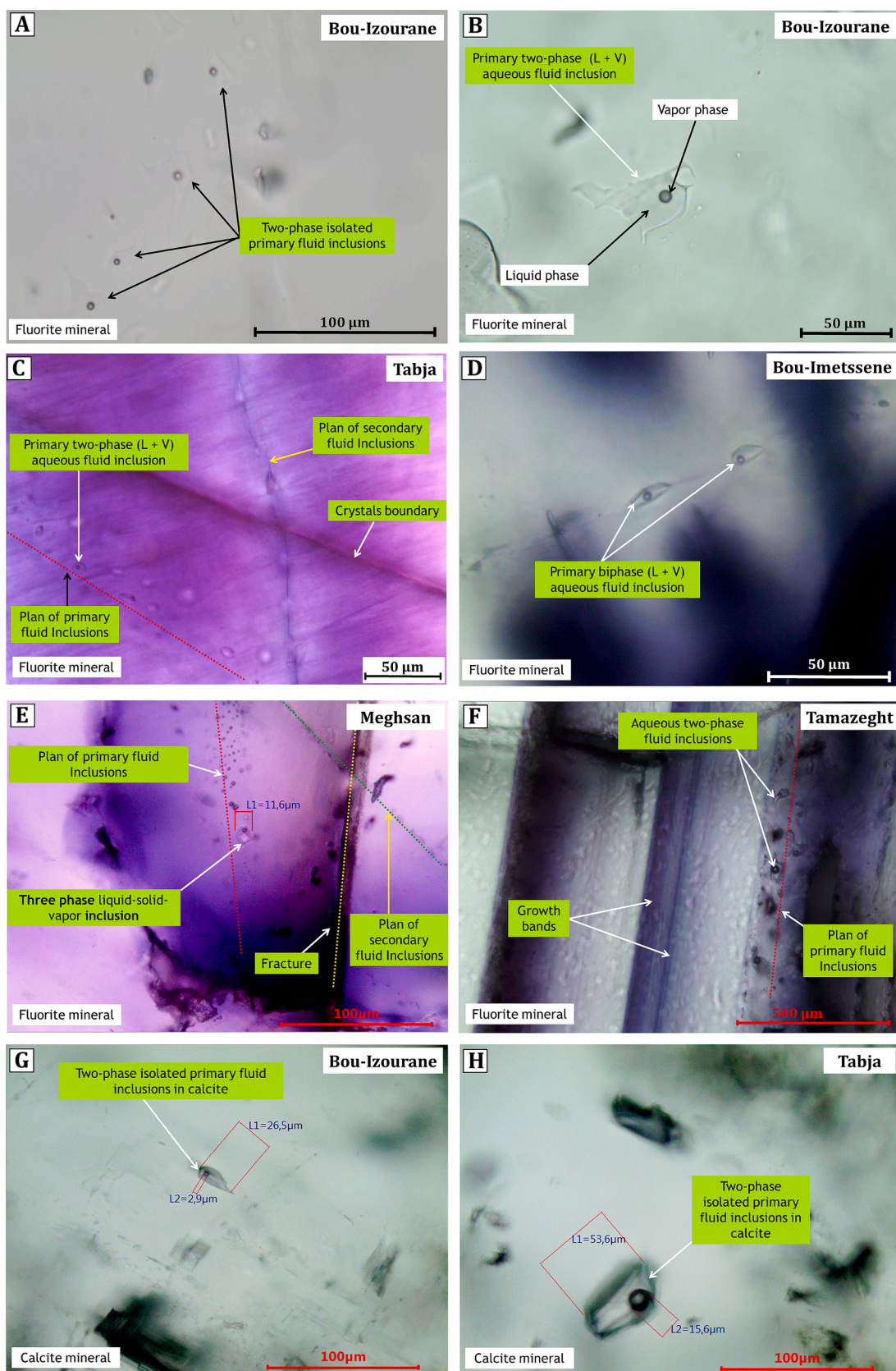


Fig. 7. Representative plane polarized light photomicrographs of thick sections showing selected petrographic relationships and types of fluid inclusions hosted in fluorite and calcite at the various sites from the Bou-Izourane district and Tamazeght complex.

Table 2

Summary of fluid inclusion microthermometric data in fluorite crystals from different sites of the Bou-Izourane district and Tamazeght complex. (N.D. – not determined).

Sample	Mineral	Inclusion type	Number	$\text{Th} (\text{°C}) \pm 1$	$\text{Tf} (\text{°C}) \pm 1$	$\text{Te} (\text{°C}) \pm 1$	$\text{Tm} (\text{°C}) \pm 0.1$	Salinity (wt % NaCleqv)
Bou-Izourane	Fluorite	Primary	23	[91 to 159]	[-42 to -39]	[-24 to -17]	[-2.1 to -0.5]	[0.8 to 3.5]
	Calcite	Primary	10	[107 to 119]	[-40 to -37]	N.D.	[-1.2 to -0.7]	[0.9 to 2.8]
Bou-Kharouba	Fluorite	Primary	14	[96 to 125]	[-39 to -36]	[-25 to -16]	[-1.3 to -0.6]	[0.9 to 2.9]
	Fluorite	Primary	15	[108 to 141]	[-42 to -39]	[-30 to -24]	[-1.8 to -0.9]	[1.5 to 3.1]
Takkat	Fluorite	Primary	58	[99 to 198]	[-43 to -38]	[-12 to -10]	[-2 to -0.7]	[1.2 to 3.4]
	Fluorite	Secondary	25	[79 to 169]	[-42 to -39]	[-14 to -9]	[-1.8 to -0.6]	[1.0 to 3]
Meghsan	Calcite	Primary	20	[110 to 142]	[-43 to -37]	N.D.	[-1.7 to -0.5]	[0.9 to 2.9]
	Fluorite	Primary	26	[169 to 241]	[-44 to -39]	[-13 to -5]	[-2.2 to -1.2]	[2.1 to 3.7]
Meghsan	Fluorite	Secondary	22	[101 to 287]	[-41 to -38]	[-11 to -5]	[-2 to -0.9]	[1.5 to 3.4]
	Tamazeght	Primary	27	[115 to 143]	[-42 to -39]	[-14 to -8]	[-1.6 to -0.1]	[0.2 to 2.7]
Bou-Imetssene	Fluorite	Primary	15	[126 to 187]	[-63 to -57]	[-23 to -21]	[-15.3 to -13.8]	[17.6 to 18.9]

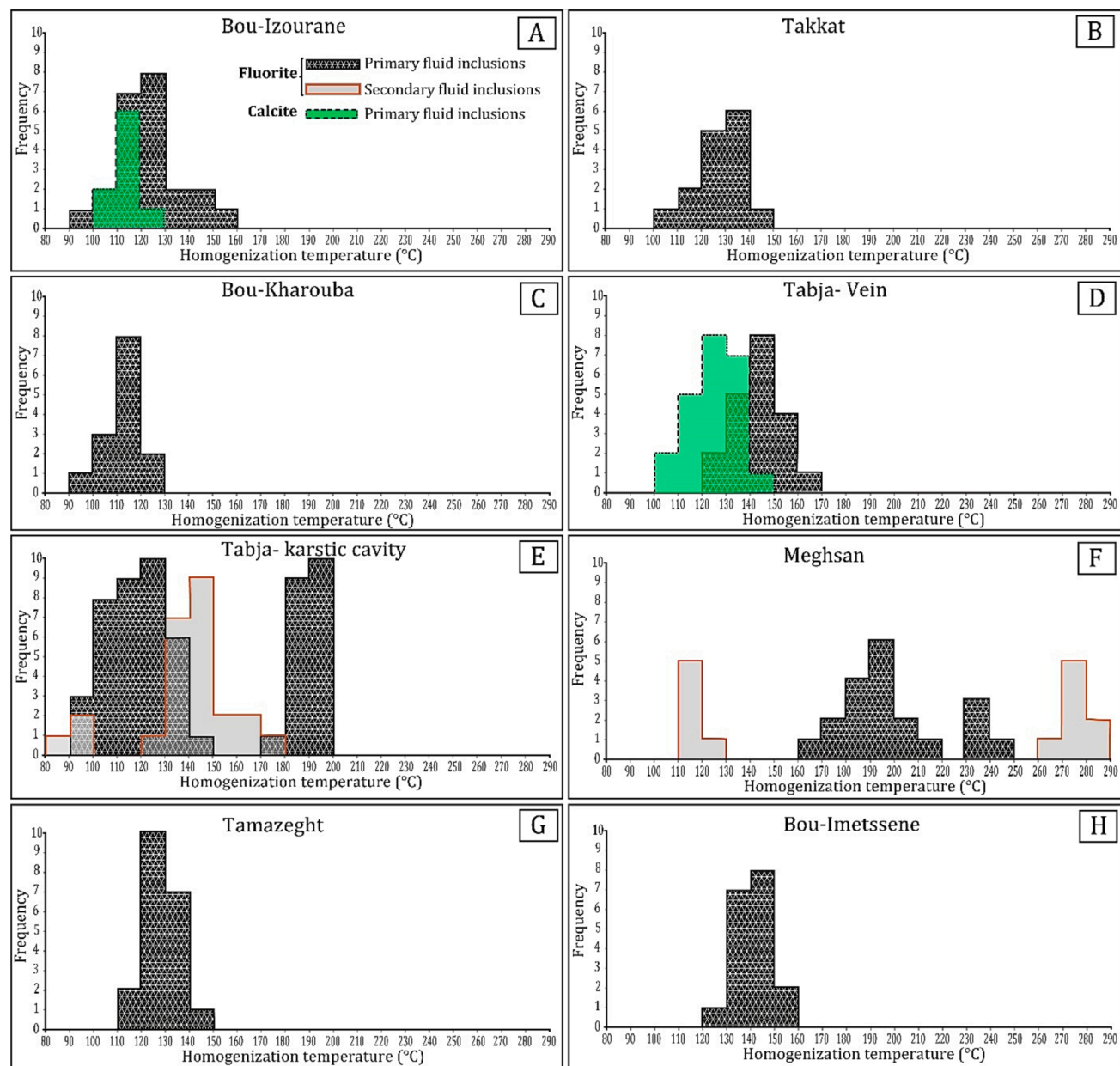


Fig. 8. Frequency histograms of homogenization temperatures for primary and secondary inclusions in fluorite and calcite crystals from Tamazeght complex and Bou-Izourane F district.

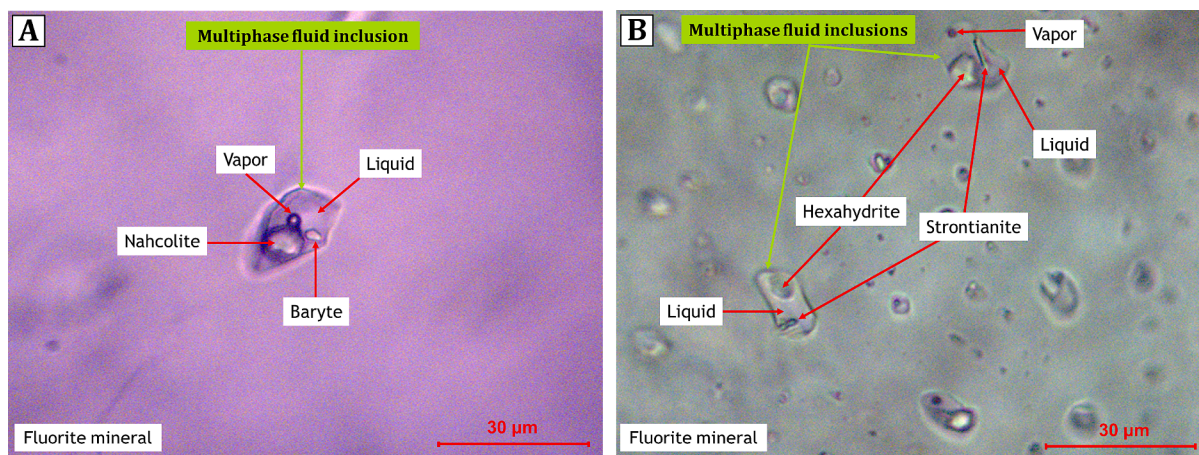


Fig. 9. Photomicrographs of multiphase fluid inclusions in Meghsan fluorite deposit.

Table 3

Isotopic compositions $\delta^{18}\text{O}$ V-PDB and $\delta^{13}\text{C}$ V-PDB of the calcite filling the fluorite fractures collected in the Tabja site (C_{Ta}) and the Bou-Izourane site (C_{Bz}).

Sample	Mineral	Th (°C)	$\delta^{18}\text{O}$ ‰ V-PDB	$\delta^{13}\text{C}$ ‰ V-PDB
Tabja	Calcite (C_{Ta})	[115 to 142]	-17.1	-0.7
Bou-Izourane	Calcite (C_{Bz})	[107 to 119]	-18.7	-0.8

- (1) An initial phase of fluorite emplacement associated with the dissolution of the host rock. Fragments of calcite from the host rock are included as enclaves in the cores of the euhedral fluorite for sites located in the sedimentary cover (Fig. 3D). For the Meghsan and Bou-Imtessene sites, the fluorite-parental fluids interacted with the syenites and almost completely replaced their primary minerals (mainly aegirine and potassium feldspars) (Figs. 6 and 5C). Some zircon crystals are very strongly dissolved in the Bou-Imtessene site with the release of Nb-U oxides, originally in inclusions in zircons (Fig. 5E, F). These undissolved Nb-U oxides produce radiation halos in the fluorite, similar to those documented by Dill and Weber, (2010) (Fig. 6C). The presence of fluorine increases the solubility of zircon and the mobility of Zr in magma-derived hydrothermal fluids in alkaline peralkaline rocks (Salvi et al., 2000; Sheard et al., 2012). At Bou-Imtessene, where zircons are highly dissolved, fluids are NaCl-rich (~18 wt% equiv. NaCl) whereas at Meghsan where fluids are much less saline (~2 wt% equiv. NaCl), zircons are preserved (Fig. 5D). The dissolution of zircon at the Bou-Imtessene site would therefore be due to the circulation of fluorine-rich saline alkaline fluids.
- (2) A phase of fracturing and clogging by calcite that partially replaces fluorite (Fig. 4A-C and 5B). In the literature (e.g., Putnis, 2009; Gigoux et al., 2016), many fluorite deposits show replacement of calcite by fluorite, but the reverse is very rarely documented. Experimental studies (e.g., Ramamohana Rao et al., 1993; Stefánsson et al., 2013; Sar et al., 2020) show that fluorite dissolution is facilitated by the presence of sodium bicarbonate, which leads to calcite precipitation under conditions of low temperatures (70–95 °C) and alkaline pH (>7). Therefore, under alkaline conditions, CaF_2 dissolves because the Ca^{2+} content in solution is limited by the precipitation of CaCO_3 in the presence of CO_3^{2-} ions (Stefánsson et al., 2013). Further dissolution of fluorite is favoured when dissolved Ca^{2+} is removed by precipitation of calcite.
- (3) The third stage consists of micro-quartz (up to 60 μm -large) and corresponds to a silicification phase that altered the fluorite and calcite crystals. The fluorite deposit of Bou-Izourane and the Tamazeght complex is added to the deposits reported worldwide

that have undergone intense silicification of the mineable minerals (Fig. 2H). Silicification may result from either late cooling of the mineralizing fluid or late circulation of a different fluid leading to the replacement of fluorite by micro-quartz (Burisch et al., 2017). Since there is no evidence of interaction between the mineralizing fluid and another fluid, we assume that silicification is controlled by the late circulation of fluids undergoing a decrease in temperature, perhaps associated with cooling of the constituent rocks of the Tamazeght complex.

- (4) A fourth stage is recognized at the Meghsan site with the precipitation of iron oxides that fill cracks intersecting fluorite and calcite.

5.2. Fluorite color insight

The origin of fluorite color has been commonly attributed to color centers (Bill, 1982; Gu et al., 2011; Aoki et al., 2015; Gaft et al., 2020), rare earth element impurities (Bill and Calas, 1978; Kempe et al., 2002; Dill and Weber, 2010), and calcium colloids (Allen, 1952; Mackenzie and Green, 1971; Braithwaite et al., 1973; Galwey et al., 1979). Fluorites from the Bou-Izourane district are predominantly light violet, lilac violet to dark violet in color. The purple to black color of the fluorite appears to be due primarily to colloidal calcium particles (Allen, 1952; Mackenzie and Green, 1971; Braithwaite et al., 1973; Galwey et al., 1979), whose size determines the color (Goebel, 1930): small particles yield green crystals, while increasing aggregate size produces blue, purple, and black crystals (Allen, 1952). The latter colors (purple to black) have also been related to radiation and mechanical damage due to radioactive inclusions, and is manifested by the irregular distribution of color “pleochroic halos” that originates from radiation (Goebel, 1930; Braithwaite et al., 1973; Vochten and Geys, 1977). The petrographic study shows that secondary purple lilac color in the form of radiation halos at the Bou-Imtessene site is related to radiation and mechanical damage caused by radioactive “uranpyrochlore” inclusions in the fluorite.

5.3. Origin of ore-forming fluids

5.3.1. Calcite stable isotopic composition

The origin of the fluids can be approximated by the O stable isotope of the mineral matrix provided that the crystallization temperatures are known. In order to interpret this data to characterize the fluids from which the fluorites originated, we assume here that the calcites and fluorites were deposited from the same fluid. This is suggested by the fact that the homogenization temperatures and fluid inclusion salinities for calcite and fluorite are of the same order and that the geochemical signatures (rare earth distributions) are also comparable.

Table 4

Elemental composition of fluorite from the different sites of the Bou-Izourane district and Tamazeght complex. bdl: below detection limit.

Site	Fluorite																				
	Bou-Imetssene (n = 20)			Bou-Izourane (n = 22)			Bou-Kharouba (n = 9)			Meghsan (n = 15)			Tabja (n = 15)			Takkat (n = 16)			Tamazeght (n = 59)		
Trace element (ppm)	Min.	Max.	Avg.	Min.	Max.	Avg.	Min.	Max.	Avg.	Min.	Max.	Avg.	Min.	Max.	Avg.	Min.	Max.	Avg.	Min.	Max.	Avg.
Mg	46	950	498	43	94	68.5	63	127	95	46	73	59.5	45	74	59.5	40	82	61	46	81	63.5
Ca	600,000	830,000	715,000	542,000	860,000	701,000	630,000	910,000	770,000	589,000	767,000	678,000	600,000	900,000	750,000	610,000	810,000	710,000	603,000	920,000	761,500
Sr	410	660	535	108	920	514	270	850	560	4900	9400	7150	38	1900	969	91	860	475.5	350	2220	1285
Y	0.38	4.5	2.44	2.39	65	33.69	22.1	67	44.55	12.2	34	23.1	0.008	6.8	3.41	2	51	26.5	0.42	76	38.21
La	1.31	17	9.15	0.078	37	18.54	0.39	17	8.69	0.118	21	10.56	0.1	11	5.55	0.5	28	14.25	0.369	39	19.68
Ce	1.44	6	3.72	0.095	23.5	11.8	0.79	13.5	7.14	0.28	42	21.14	0.12	5.9	3.10	1.03	46	23.51	0.085	27	13.5
Pr	0.131	19.7	9.92	0.035	1.65	0.84	0.2	2.4	1.29	0.059	1.24	0.65	0.01	0.93	0.47	0.113	9.6	4.86	0.0127	8.1	4.06
Nd	0.25	39	19.62	0.222	6.7	3.46	2	10.9	6.45	0.25	3.9	2.08	0.008	3.05	1.52	0.54	38	19.27	0.075	25.6	12.84
Sm	0.014	5.2	2.61	0.033	1.9	0.97	1.35	6	3.675	0.211	1.17	0.69	bdl	0.58	0.29	0.063	5	2.53	0.013	4.6	2.31
Eu	0.007	1.22	0.61	0.015	0.8	0.41	0.33	1.34	0.835	0.087	0.558	0.32	bdl	0.158	0.08	0.02	1	0.51	0.0077	1.41	0.71
Gd	0.012	3.08	1.54	0.096	3.6	1.85	1.88	8.7	5.29	0.303	2.5	1.40	bdl	1.29	0.65	0.055	4.1	2.08	0.035	6	3.02
Tb	bdl	0.39	0.19	0.012	0.45	0.23	0.27	1.8	1.035	0.057	0.45	0.25	bdl	0.161	0.08	0.015	0.64	0.33	0.0047	1.04	0.52
Dy	bdl	2.2	1.10	0.082	3.5	1.79	1.67	8.2	4.935	0.38	4	2.19	bdl	1.4	0.7	0.08	4	2.04	0.0103	9	4.51
Ho	bdl	0.37	0.18	0.03	0.84	0.43	0.45	2	1.225	0.067	0.65	0.36	bdl	0.35	0.17	0.039	0.95	0.49	0.0026	2.41	1.21
Er	bdl	1.78	0.89	0.069	2.7	1.38	1.1	4.5	2.8	0.283	2.08	1.18	bdl	1.14	0.57	0.07	2.67	1.37	0.0055	6.5	3.25
Tm	bdl	0.2	0.10	0.005	0.51	0.26	0.127	0.77	0.448	0.036	0.3	0.17	bdl	0.127	0.06	0.0117	0.33	0.17	0.0011	1.8	0.90
Yb	bdl	2.33	1.16	0.066	2.9	1.48	0.66	3.7	2.18	0.238	1.83	1.03	bdl	0.91	0.45	0.082	2.02	1.05	0.016	5.3	2.65
Lu	bdl	1.1	0.55	0.008	0.46	0.24	0.07	0.6	0.335	0.03	0.23	0.13	bdl	0.151	0.075	0.007	0.29	0.15	0.001	0.77	0.38
Th	bdl	0.6	0.3	bdl	8.4	4.2	1.04	9.8	5.42	bdl	1.5	0.75	bdl	1.8	0.90	0.5	6.3	3.4	0.49	6.5	3.49
U	bdl	0.69	0.35	bdl	0.071	0.038	0.009	0.098	0.05	bdl	0.034	0.017	bdl	0.19	0.095	0.007	0.083	0.045	0.091	0.72	0.405
Tb/Ca	8.28E-11	4.75E-07	6.44E-08	1.84E-08	5.63E-07	1.61E-07	3.82E-07	2.27E-06	8.45E-07	8.63E-08	6.82E-07	1.99E-07	4.66E-09	2.33E-07	5.95E-08	2 E-07	9.27E-07	4.46E-07	6.31E-09	1.54E-06	7.23E-07
Tb/La	3.48E-05	0.016030	0.00397428	0.0014159	0.37003	0.05564	0.01594	1.45038	0.47347	0.0033333	0.89830	0.1989190	0.0015328	0.28571	0.05599	0.00185	1.16	0.14145	0.00030	1.0298	0.16259
Y/Ho	22.12	258.82	131.03	35.75	134.67	76.85	44.91	65.33	54.55	93.39	182.09	130.27	37.39	93.10	58.48	42.25	73.87	57.54	27.44	68.46	50.94
ΣREE	4.02	573.06	61.53	2.2304	54.98	18.34	13.324	57	33.04	4.091	70.91	13.06	0.60	20.86	5.89	3.1229	124.39	33.58	7.756	263.13	45.84
ΣLREE	4	572.07	60.85	0.7475	54.32	15.64	8.86	42.4	23.9	1.994	61.37	10.16	0.49	17.05	4.97	2.781	122.74	28.18	6.159	259.35	35.42
ΣHREE	0.009	7.71	0.69	0.316	11.36	2.69	4.464	21.57	9.15	1.25	9.54	2.89	0.01	3.95	0.92	0.3419	10.69	5.39	0.0412	24.17	10.42

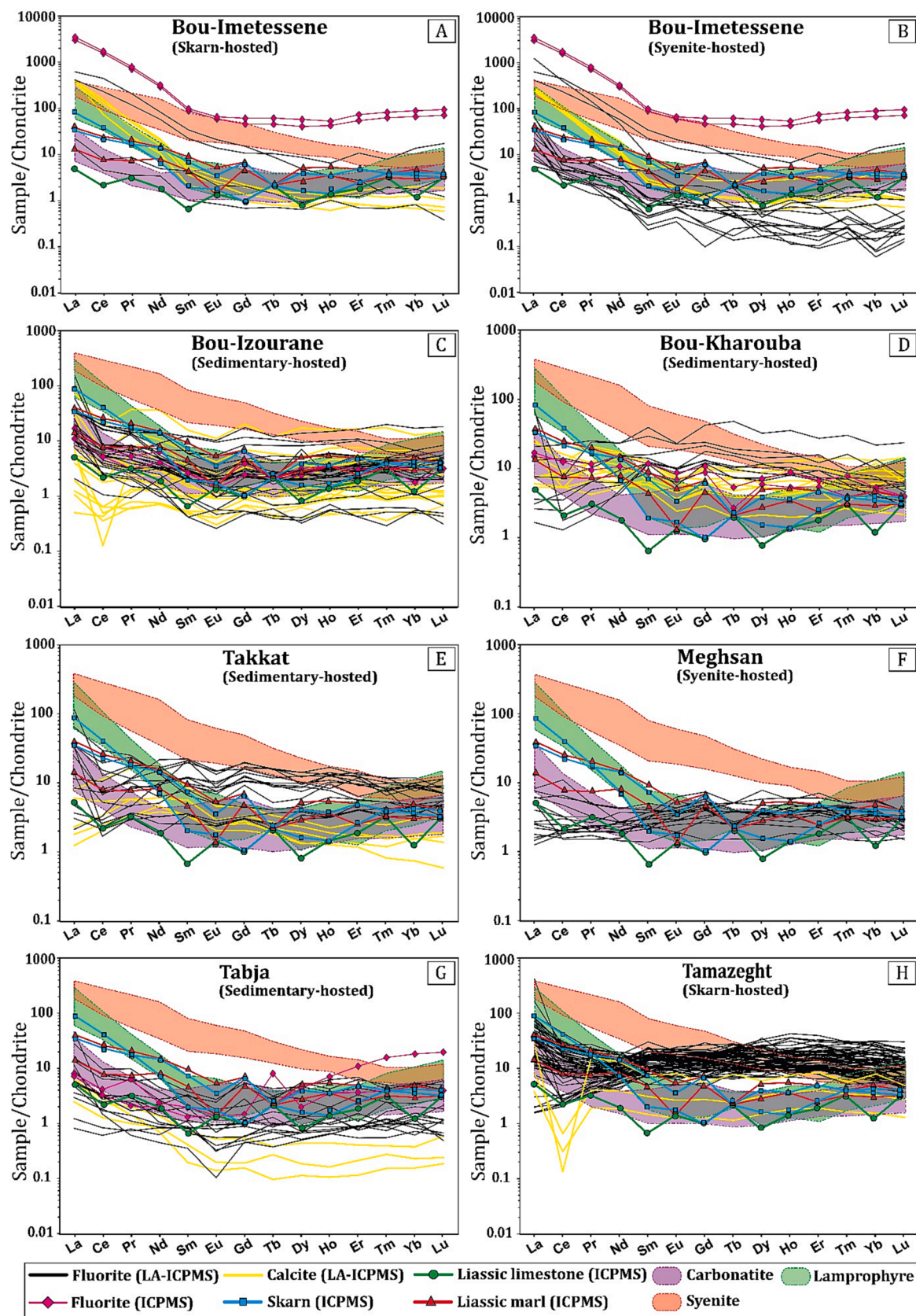


Fig. 10. Chondrite-normalized REE patterns of fluorites, calcites and hosted rocks at sites in the study area (Sun and McDonough 1989). (A, B). Bou-Imetessene. (C) Bou-Izourane. (D) Bou-Kharouba. (E) Takkat. (F) Meghsan. (G) Tabja. (H) Tamazeght.

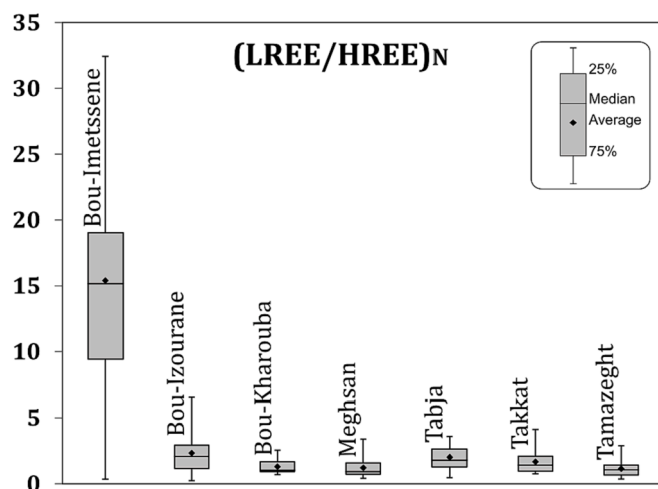


Fig. 11. Box-whisker diagram of (LREE/HREE)_N fractionation for the fluorite from sites in the Bou-Izourane region and Tamazeght complex. N: Normalization to chondrite (Sun and McDonough, 1989).

The measured Th of the Tabja calcite and Bou-Izourane calcite corresponds to the minimum temperature at which the fluid inclusions were trapped. However, a pressure correction must be applied to determine the trapping temperature (T_t) of the fluid inclusions, which also corresponds to the crystal growth temperature in the absence of post-trapping deformation (Goldstein and Reynolds, 1994). Pressure correction requires an estimate of the fluid entrapment pressure. Exhumation rates derived from low-temperature thermochronology in the Central High

Atlas, estimated at ~ 0.05 km/Ma (Lanari et al., 2020), indicate that burial in the Bou-Izourane district has never exceeded 2 km since the emplacement of the middle Eocene Tamazeght magmatic intrusion (44 ± 4 Ma; Tisserant et al., 1976). Assuming that the Lower Jurassic in the study area is generally under a hydrostatic pressure regime (hydrostatic gradient of 100 bar/km), the maximum trapping pressure is about 200 bar. The trapping temperature of fluid inclusions in the Tabja calcite is then estimated at ~ 143 ± 8 °C, and ~ 122 ± 3 °C in the Bou-Izourane calcite (Fig. 14A). Thus, using these trapping temperatures, the calculated δ¹⁸O values of mineralizing fluids for the Tabja site are between – 5.5 ‰ and – 1.6 ‰ V-SMOW (av. – 3.6 ‰ V-SMOW, Fig. 14B). For Bou-Izourane, the δ¹⁸O values of the parent fluid are between – 3.3 ‰ and – 2 ‰ V-SMOW (av. – 2.6 ‰ V-SMOW, Fig. 14B). The average δ¹⁸O values of the parent fluid are therefore very close (Fig. 14B). These compositions reflect a dominant meteoric origin (Fig. 15A), consistent with the low salinities of the fluid inclusions, with the exception of Bou-Imtessene.

5.3.2. Fluorite

Most carbonatite-related fluorite mineralizations in the world that have been interpreted as being derived from late-magmatic fluids (Amba Dongar, India, Palmer and Williams-Jones, 1996; Itapirapuá, Brazil, Andrade et al., 1999; Okorusu, Namibia, Bünn et al., 2002), show wide ranges of homogenization temperatures (100 to 500 °C) and salinities. Therefore, low-temperature, low-salinity fluid inclusions in fluorites derived from late-magmatic fluids have been considered to reflect a mixture between a late-magmatic F-bearing fluid and meteoric water (Simonetti and Bell, 1995; Palmer and Williams-Jones, 1996). Common daughter minerals in fluid inclusions hosted in fluorite are carbonates, strontianite, nahcolite, shortite, sulfates, and alkali, alkaline earth and

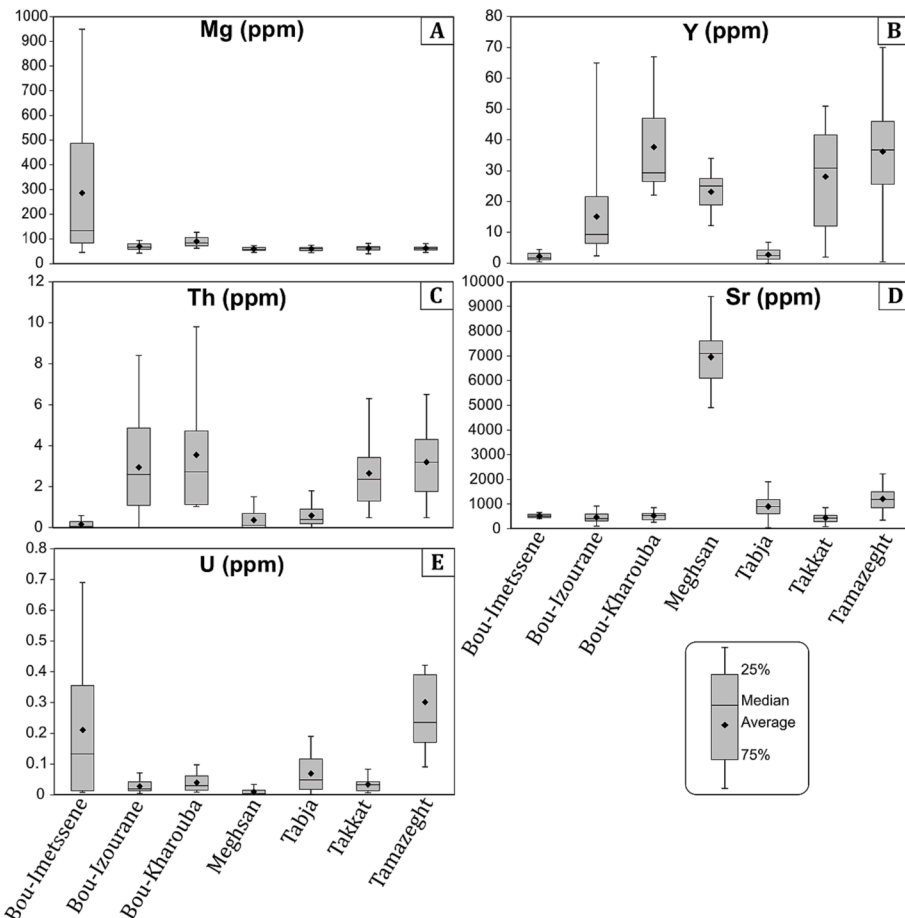


Fig. 12. Box-whisker diagram of trace element concentrations for the fluorite from sites in the Bou-Izourane region and Tamazeght complex.

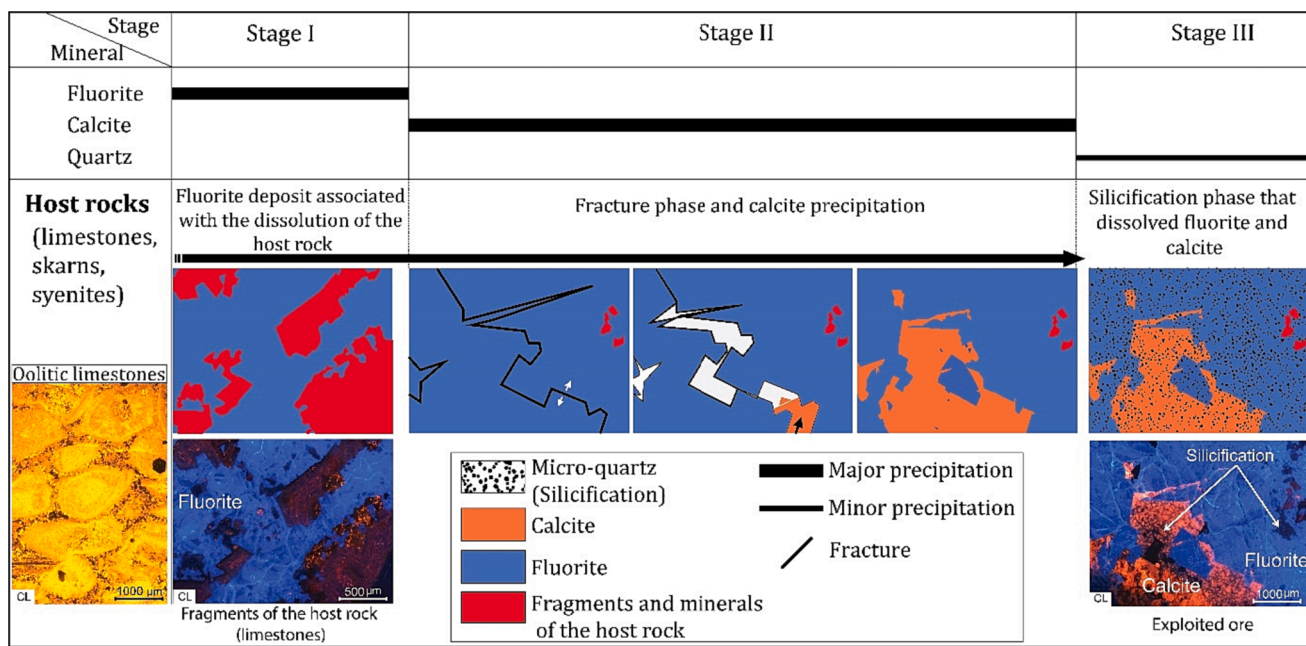


Fig. 13. General paragenetic sequence of the fluorite deposits of the Bou-Izourane district and Tamazeght complex.

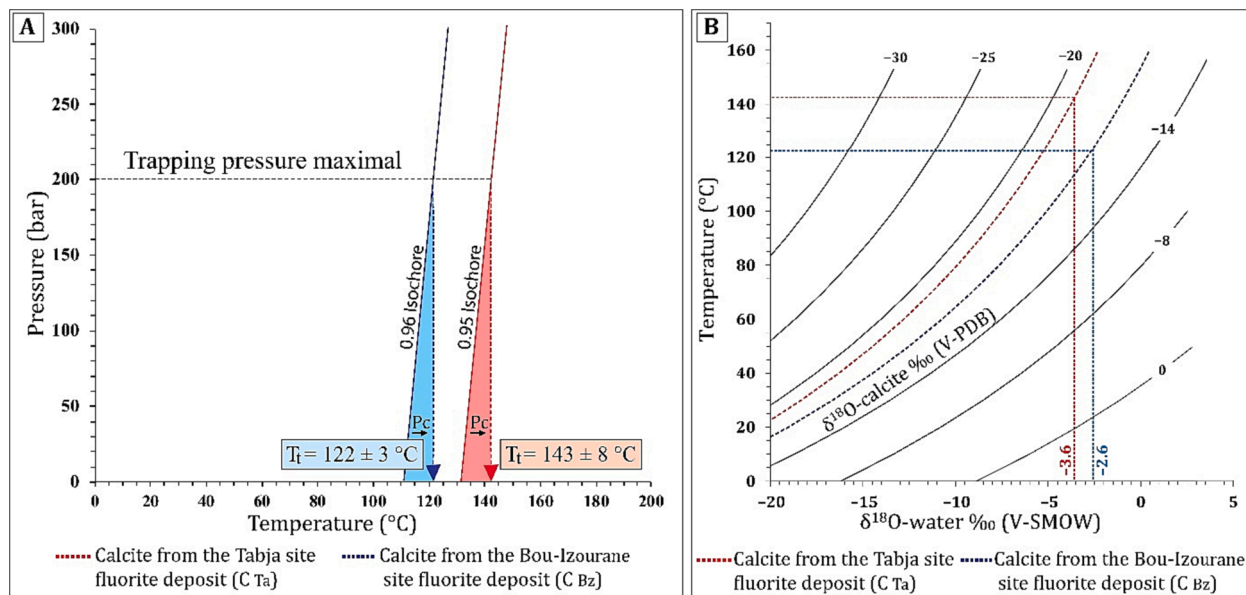


Fig. 14. (A). Pressure correction (Pc) applied on fluid inclusions hosted in calcites from the Bou-Izourane district to calculate the trapping temperature (Tt); (B). Oxygen isotopic values of calcite associated with fluorite plotted on the temperature-dependent, calcite-water oxygen fractionation curve of Zheng (1999).

rare earth chlorides. Carbon dioxide is frequently detected in the vapour phase (Palmer and Williams-Jones, 1996; Xu et al., 2012; Redina et al., 2020; Bühn et al., 2002; Kynicky et al., 2019; Öztürk et al., 2019; Rankin et al., 2003; Smith et al., 2015; Redina et al., 2021; Prokopyev et al., 2020).

Raman spectroscopy, microthermometry data of fluid inclusions (Th and Tm) and oxygen isotope compositions obtained in the calcite from the Bou-Izourane district show two origins for the fluorite. Fluorite mineralizing fluids from sites hosted in Liassic carbonate rocks (i.e., Bou-Izourane, Bou-Kharouba, and Takkat), with the exception of Tabja, have low salinities (1.5 to 3 wt% NaCl equiv.). This suggests a primary contribution of meteoric waters. The Tamazeght complex then acts as a heat source.

The Tamazeght site hosted in skarns to the NW of the Tamazeght complex, the Tabja site in Liassic carbonate rocks, and the Meghsan site hosted in Tamazeght syenites to the SE of the complex, are characterized by the same range of salinity as the other sites, but with a slight rise in temperature centred around 160 °C. Fluorites in the latter three sites exhibit fluid inclusions containing nahcolite (NaHCO_3), calcite and strontianite (SrCO_3), and are sometimes rich in dissolved CO_2 . This reflects the participation of late-magmatic fluid in the precipitation of fluorite at these three sites.

For Bou-Imtessene, the mineralizing fluids have temperatures close to those of the other sites, but the salinity is very high, reaching 18 wt% NaCl equiv. (Fig. 15B). Several phenomena are commonly invoked to explain high NaCl contents in geofluids: (1) basinal brine percolation

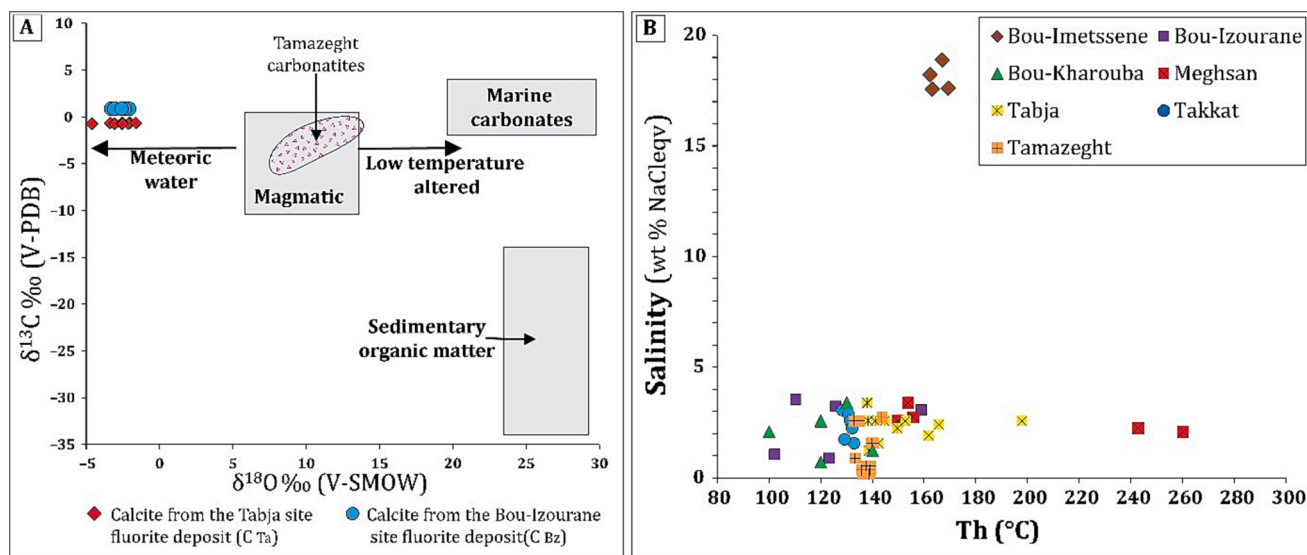


Fig. 15. (A). $\delta^{18}\text{O}$ versus $\delta^{13}\text{C}$ diagram of calcites from the Bou-Izourane district. The fields for marine carbonates, magmatic and sedimentary organic matter are after Liu et al., 2007; Tamazeght (Tamazert) carbonatites is from Bouabdellah et al., 2010b; (B). Homogenization temperature (Th) versus salinity diagram of primary fluid inclusions of fluorite crystals from the Bou-Izourane district and Tamazeght complex.

(Sizaret et al., 2004), (2) local dissolution of evaporitic minerals (Bakelli et al., 2022; Boiron et al. 2002), (3) boiling processes (Darinont and Coipel, 1982; Sizaret et al., 2004) and (4) participation of late-magmatic fluids (Palmer and Williams-Jones, 1996; Bühl et al., 2002; Redina et al., 2021). As the presence of evaporites is not mentioned locally, and in the absence of boiling markers in the fluid inclusion record, we propose a local concentration of NaCl by late-magmatic fluids and/or the interaction between the mineralizing fluid and Na- and Cl-rich syenite minerals (albite, sodalite, biotite and amphibole) (Wang et al., 2016).

5.4. Evidence of fluid-rock interactions

Salvi et al. (2000) demonstrated that high field strength elements (HFSE), specifically REE, Zr, Ti, and Nb, are mobilized during a short duration and spatially limited hydrothermal alteration in the nepheline syenites and pegmatites of Tamazeght. The mobilization of these HFSE occurs through OH-F complexation, which requires a fluid with a high concentration of fluorine (F) and a temperature of about 300 °C, with the quasi-total absence of calcium (Ca). This phenomenon is explained by the presence of F-rich residual brine (25 wt% equiv. NaCl) exsolved from the most evolved Tamazeght pegmatites, which leaches HFSE (Salvi et al., 2000). These considerations mainly indicate that the magmatic-hydrothermal activity associated with the emplacement of the Tamazeght complex during the Eocene is a potential source of fluorine.

Petrographic observations show dissolution of primary minerals (mainly aegirine and K-feldspars) from syenites of the Tamazeght complex (Fig. 5C and 6B, F), and calcite from other country rocks in the Bou-Izourane district (Appendix A (Fig. A.4)). The source of F could be from fluid-rock interactions, as apatite, biotite, and amphibole minerals in most rocks of the Tamazeght complex are halogen-rich and have higher F contents in the more evolved rocks (i.e., syenites) (Wang et al., 2016). The higher Sr content in fluorite from the Meghsan site may most likely be due to the reaction of mineralizing fluids with carbonatites and calcite dissolution. The interaction of F-rich fluids with the host rocks may be the source of the calcium.

The representation of fluorite samples in the Tb/Ca and Tb/La diagram, where three genetically distinct domains can be identified (Möller et al. 1976; Möller and Morteani, 1983, Möller, 1983), indicates the hydrothermal field for fluorites in the Bou-Izourane district and the Tamazeght complex (Fig. 16A). A few rare analyses from the Bou-

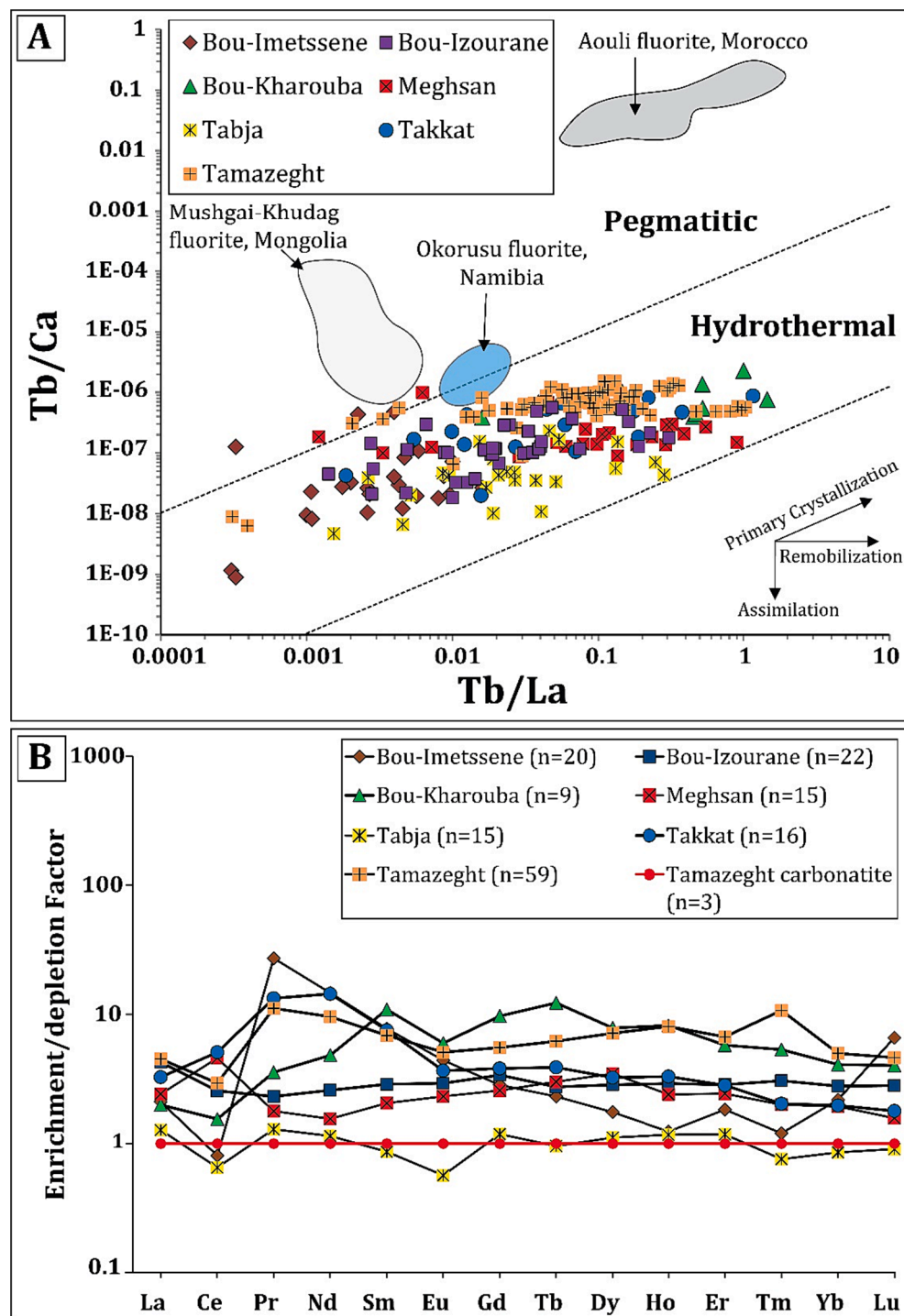
Imetssene, Meghsan and Tamazeght sites fall into the pegmatitic field. This overlap on the pegmatitic field, for Bou-Imetssene and Meghsan hosted in syenites, could be attributed to local interactions between the fluid and the syenites of the Tamazeght complex and/or to the participation of late magmatic fluids. This is also the case for the Mushgai-Khudag fluorite in Mongolia (Redina et al., 2020) and the Okorusu fluorite in Namibia (Bühl et al., 2002), which have been interpreted as late-magmatic (carbonatitic) in origin, and the Aouli fluorite in Morocco (Margoum et al., 2015), which has been shown to be precipitated not as a result of purely magmatic fluid involvement but by hot basin-derived brines and fluid-rock interaction at high fluid-rock ratios. This explains that all fluorites from these deposits fall into the pegmatitic domain (Fig. 16A).

Despite the difference in the relative rare earth element enrichment/depletion factor in the fluorites of the Bou-Izourane district and Tamazeght complex compared to the Tamazeght carbonatite, the REE distributions are flat-lying when normalized to carbonatites and broadly similar (Fig. 16B). This again reflects the involvement of carbonatitic fluids associated with late magmatic activity and/or the interaction of mineralizing fluids at depth with the Tamazeght magmatic complex carbonatites. These results point to two possible sources (meteoric and late magmatic) for the fluorites of the Bou-Izourane district and the Tamazeght complex.

The fluorine in the syenite-hosted fluorite of Bou-Imetssene is derived from the dissolution and replacement of the syenites. The penetration of meteoric fluids in the system constitutes the final stage of the late magmatic-hydrothermal history of Tamazeght (Schilling et al., 2009). During this period, heated meteoric fluids precipitated fluorite in Liassic carbonates (i.e., Bou-Izourane, Bou-Kharouba, and Takkat). These fluids were enriched in fluorine by leaching the syenites, lamprophyres, and probably other F-rich igneous rocks.

5.5. Genetic model

The (U-Th)/He and AFT ages in the central High Atlas reveal that these regions were at temperatures below ~ 70–110 °C since the Mesozoic (Barbero et al., 2007). These maximum burial temperatures are lower than the homogenization temperatures of the fluid inclusions. This implies either the existence of an anomalously high geothermal gradient or fluids expelled from deeper levels not being in thermal equilibrium with the surrounding rocks. Since the mineralized fractures



cut through the Tamazeght Complex rocks, and fluorite replaces the constituent minerals of the syenites, fluorite mineralization in the Bou-Izourane district and the Tamazeght Complex occurred after the Tamazeght Complex was emplaced (Fig. 17A). The Tamazeght complex likely played a role in increasing the local geothermal gradient, potentially leading to the development of local-scale convection cells, and this acted as a potential heat source and driving mechanism to move mineralizing fluids to the surface, which is similar to the case of the El Hammam fluorite deposit in Morocco (Bouabdellah et al., 2010a) and the Inner Mongolia fluorite deposit (Pei et al., 2017).

Fluorites characterized by high salinity (18 wt% NaCl equiv.) aqueous inclusions containing calcite (i.e., Bou-Imtessene) and low

salinity fluid inclusions (1.5–3 wt% NaCl equiv) containing daughter minerals such as nahcolite, strontianite and rich in dissolved CO_2 (i.e., Meghsan, Tamazeght and Tabja), and which have homogenizing temperatures centred around $160 \pm 30^\circ\text{C}$, may be of meteoric origin but associated with late magmatic activity following the emplacement of Tamazeght carbonatites. At sites hosted in Liassic carbonate rocks (i.e., Bou-Izourane, Bou-Kharouba, and Takkat), the fluorite contains two-phase aqueous inclusions, showing median Th around 130°C and low salinities of 1.5–3 wt% NaCl equiv., suggesting a meteoric origin, supported by oxygen isotope compositions obtained in the calcite.

These results point to the direct involvement of carbonatitic fluids from the middle Eocene Tamazeght magmatic complex in the fluorite

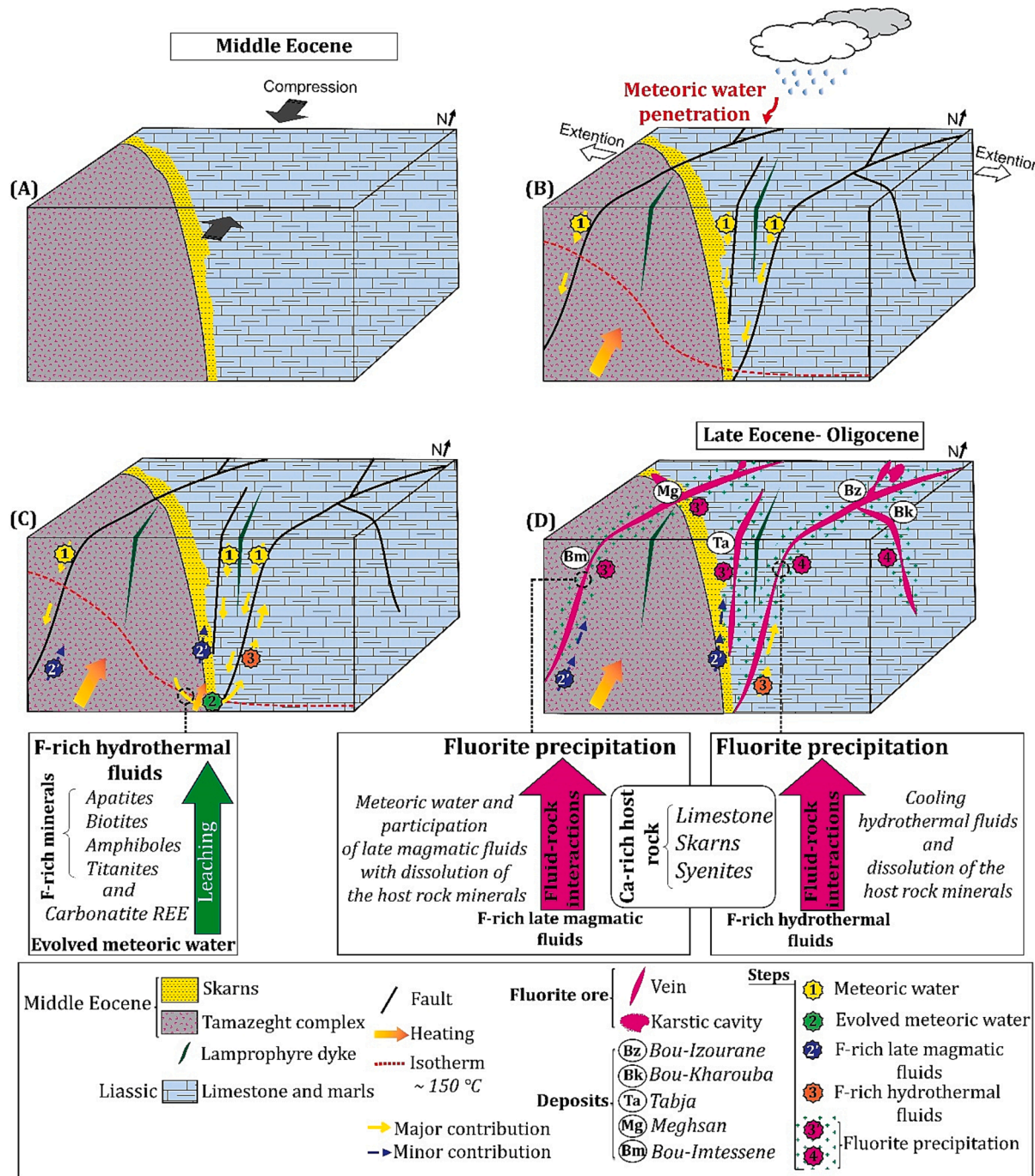


Fig. 17. Conceptual model proposed of the Tamazeght complex and Bou-Izourane district fluorite hydrothermal deposit. (A) The Tamazeght complex intrudes Ca-rich sedimentary rocks (limestones and marls); (B) Fault reactivation inherited from the Atlasic rifting followed by the emplacement of the lamprophyres of the Bou-Izourane district and by the per descensum circulation of meteoric waters at the interface between the intrusion and the sedimentary formations; (C) Step 2 and 3: The meteoric water heated by the intrusion ascended along the brittle faults, resulting in F-leaching from the apatite, biotite, titanite and amphibole minerals during the circulation of hydrothermal fluids in contact with the carbonatite and other rocks of the Tamazeght intrusion; Step 2': The per ascensum circulation of the F-rich late magmatic fluids. (D) Step 4: The interaction of the F-rich hydrothermal fluid with the Ca-rich host rock (limestones), leads to the precipitation of fluorite in the cavities, along the stratiform joints and faults; Step 3': Mixing of the meteoric water and of late magmatic fluids with dissolution of the Ca-rich host rock (limestones, skarns, syenites), leads to the precipitation of fluorite in the cavities and along faults.

mineralization just proximal to the Tamazeght complex (i.e., Bou-Imtessene, Meghsan, Tamazeght and Tabja). Mixing of meteoric fluids with the last remnants of late-magmatic F-rich brines and dissolution of the host rock (limestones, skarns, syenites, carbonatites), causes the deposition of large amounts of fluorite at the interaction site (Step2' and Step3'; Fig. 17C, D). However, no evidence of these late-magmatic fluids is detected for the fluorite mineralization hosted in the Liassic marl and

carbonate rocks (Bou-Izourane, Bou-Kharouba, and Takkat). The Tamazeght igneous complex is composed of plutonic rocks, with F (fluorine) contents as high as 0.02–0.8 wt%, and distributed in minerals as follows: apatites (2.3–3.4 wt% F), biotites (0.2–2.6 wt% F), amphiboles (0.1–1.1 wt% F) and titanites (0.03–0.8 wt% F) (Wang et al., 2016). The Tamazeght complex could have been a potential source of F for fluorite mineralization at the Bou-Izourane, Bou-Kharouba, and Takkat sites by

leaching fluorine from these minerals during circulation of hydrothermal fluids in contact with carbonatites and other rocks of the Tamazeght intrusion (Step2; Fig. 17C). This step takes place after the *per descensum* circulation of meteoric waters potentially at the interface between the intrusion and the sedimentary formations (Step1; Fig. 17B). Indeed, the origin of the fluorite mineralization at Bou-Izourane, Bou-Kharouba, and Takkat would be the result of circulation of fluorine-rich hydrothermal fluids guided by the brittle structures acquired during Triassic-Jurassic rifting (Step3; Fig. 17C, D). The interaction of the hydrothermal fluid with the Ca-rich host rock (limestones) leads to the precipitation of fluorite in the cavities along the stratiform joints and faults (N20, N50-80 and N120) cutting the Liassic formations (Step4; Fig. 17D).

6. Conclusions

The fluorite deposits in the Bou-Izourane district and the Tamazeght complex in the central High Atlas of Morocco, are characterized by vein-like (N20, N50-80 and N120), stratiform and karst cavities mineralization, and are associated with sedimentary rocks (limestones and marls) of the Liassic (Bou-Izourane, Takkat, Bou-Kharouba and Tabja), with magmatic rocks (Bou-Imetssene and Meghsan) and also with skarn (Tamazeght). Even if some differences in colour and texture exist between the different sites of the Bou-Izourane district and the Tamazeght complex, the general paragenesis of these fluorite mineralizations includes three stages; (1) a first stage of fluorite emplacement associated with the dissolution of the host rock, (2) a phase of fracturing and clogging by calcite, and (3) a third stage constituted by micro-metric quartz and corresponding to a phase of silicification that altered the fluorite crystals. In the Bou-Imetssene and Meghsan sites, the fluorite veins intersect the Middle Eocene Tamazeght syenites and the mineralizing fluids that precipitated this fluorite interacted with these syenites. This indicates that these fluorite mineralizations were deposited clearly for these two sites but also for all the sites that show some similar characteristics - during the period following the establishment of the Tamazeght complex. Fluid inclusions in fluorite hosted in Liassic carbonate rocks (Bou-Izourane, Bou-Kharouba, and Takkat) are aqueous inclusions with low homogenization temperatures (~ 130 °C) and low salinities (1.5 ~ 3 wt% NaCl equiv.).

Fluorite in the Tabja, Tamazeght, Meghsan and Bou-Imetssene sites shows aqueous inclusions at slightly higher homogenization temperatures (99 °C and 241 °C) and similar low salinities as the previously mentioned sites, except for the Bou-Imetssene site which is characterized by a high salinity (~18 wt% NaCl equiv.). Multiphase inclusions containing daughter minerals of nahcolite, calcite, strontianite with a CO₂-rich vapour phase are also present in the fluorites of these last four sites. The $\delta^{18}\text{O}$ values of the fluids that precipitated fluorite-associated calcites from Tabja (highest Th) and Bou-Izourane (lowest Th), from – 5.5 to – 1.6 % V-SMOW and – 3.3 % and – 2 % V-SMOW, respectively, suggest a meteoric origin. Combining the microthermometric data and the geochemical composition, it can be concluded that the fluorites from Tabja, Tamazeght, Meghsan and Bou-Imetssene, were precipitated as a result of the participation of late-magmatic F-bearing fluids with meteoric waters. Calcite precipitated in fractures that cut the fluorite in the Bou-Izourane area and the Tamazeght complex as well as the fluorites at the Bou-Izourane, Bou-Kharouba, and Takkat sites share a common meteoric hydrothermal origin. The magmatic rocks of the Tamazeght complex, rich in halogens, are the most likely sources of fluorine. The local thermal anomaly (Tamazeght magmatism) may be the source of heat and the driving force for the percolation of mineralizing fluids through faults that cut the region to the surface. Fluid-rock interaction between F-rich fluids and the host rocks of the Bou-Izourane, Bou-Kharouba, and Takkat fluorite deposits led to the extraction of Ca from the host rocks, followed by a drop in temperature and pressure, resulting in the precipitation of fluorite.

The proposed conceptual model for the fluorite deposit formation in the Bou-Izourane district provides valuable insights that can guide exploration efforts. The fluorites hosted in the Liassic formation represent the most profitable and economical fluorite ore reserves in the Bou-Izourane region in terms of both volume and the cost of mining and processing fluorite. The silicification of fluorite negatively affects the mining potential of the Bou-Izourane district and the Tamazeght complex and reduces the grade by dissolution of the ore, thus increasing the hardness of various mineralized forms. The presence of major NE-SW trending faults, directly related with the Tamazeght magmatic complex which serves as a source of fluorine and heat, plays a crucial role in the circulation of ore-forming fluids. These faults, inherited from the Triassic-Jurassic rifting, not only facilitate fluid movement but also supply other fault systems (N20 and N120) as well as cavities found in the Liassic carbonate rocks of the Bou-Izourane area, which serve as a source of calcium. As a result, these faults and cavities represent favorable zones for the precipitation of fluorite and are highly promising targets for exploration efforts. By focusing exploration activities on these areas, there is a greater likelihood of discovering potential fluorite deposits. Future research should be conducted to date fluorite mineralizations in order to situate their genesis into the geodynamic history of the central Moroccan High Atlas.

Declaration of Competing Interest

The authors declare that they have no known competing financial interests or personal relationships that could have appeared to influence the work reported in this paper.

Data availability

Data will be made available on request.

Acknowledgments

This work is part of the results of the collaborative project PHC Toubkal N° TBK/20/110 – Campus France Maroc N°43705TG “Origine des minéralisations à fluorine de Bou-Izourane (Tamazeght, Haut Atlas Central Marocain)” between the University Mohammed I, Morocco and the University Paris-Saclay, France. The authors would like to express their gratitude to the members of “Global Mines”, for facilitating the field data collection process. C. Boukari, S. Courba, and S. Boudrif deserve special mention for their assistance with field support, photography, and sample preparation. We are grateful to S. Miska and J. Nouet for assistance with SEM, F. Haurine for assistance during LA-ICP-MS analyses, and M.-C. Caumon for Raman spectroscopy analyses. We also express our gratitude to Y. Missenard and B. Saint-Bezar from the University of Paris-Saclay and P. Boulvais from the University of Rennes for many insightful discussions. We would like to thank the anonymous reviewers for their constructive criticism and suggestions to improve the manuscript.

Appendix A. Supplementary data

Supplementary data to this article can be found online at <https://doi.org/10.1016/j.oregeorev.2023.105596>.

References

- Achmani, J., 2017. Etude des minéralisations fluorées de la région de Bou-Izourane (Haut Atlas Oriental, Maroc). Unpublished Masters, Faculté des Sciences, Casablanca, pp. 61 (in French).
- Achmani, J., Chraibi, I., Blaise, T., Barbarand, J., Brigaud, B., Bounajma, H., 2020. Virtues of fluorite-case of Bou-Izourane fluorite. Mater. Today.. Proc. 31, S114–S121. <https://doi.org/10.1016/j.matpr.2020.06.396>.

- Agard, J., 1973. Carte géologique du complexe de roches alcalines des carbonatites de Tamazeght (Haut Atlas de Midelt Maroc). Notes et Mémoires du Service Géologique du Maroc 248.
- Ait Addi, A., Chafiki, D., 2013. Sedimentary evolution and palaeogeography of mid-Jurassic deposits of the Central High Atlas. Morocco. *J. Afr. Earth Sci.* 84, 54–69. <https://doi.org/10.1016/j.jafrearsci.2013.04.002>.
- Ait Brahim, L., Chotin, P., Hinaje, S., Abdelouafi, A., El Adraoui, A., Nakcha, C., Dhont, D., Charroud, M., Sossey Alaoui, F., Amrhar, M., Bouaza, A., Tabyaoui, H., Chaouni, A., 2002. Paleostress evolution in the Moroccan African margin from Triassic to Present. *Tectonophysics* 357, 187–205. [https://doi.org/10.1016/s0040-1951\(02\)00368-2](https://doi.org/10.1016/s0040-1951(02)00368-2).
- Allen, R.D., 1952. Variations in chemical and physical properties of fluorite. *Am. Mineral.* 37 (11–12), 910–930.
- Alvaro, J.J., Ezzouhairi, H., Ayad, N.A., Charif, A., Popov, L., Ribeiro, M.L., 2008. Short-term episodes of carbonate productivity in a Cambrian uplifted rift shoulder of the Coastal Meseta Morocco. *Gondwana Res.* 14 (3), 410–428. <https://doi.org/10.1016/j.gr.2008.04.003>.
- Andrade, F.R.D., Möller, P., Lüders, V., Dulski, P., Gilg, H.A., 1999. Hydrothermal rare earth elements mineralization in the Barra do Itapirapuá carbonatite, southern Brazil: Behaviour of selected trace elements and stable isotopes (C, O). *Chem. Geol.* 155 (1), 91–113. [https://doi.org/10.1016/S0009-2541\(98\)00143-0](https://doi.org/10.1016/S0009-2541(98)00143-0).
- Aoki, T., Garvie, L.A.J., Rez, P., 2015. Observation of color center peaks in calcium fluoride. *Ultramicroscopy* 153, 40–44. <https://doi.org/10.1016/j.ultramic.2015.02.007>.
- Bakelli, A., Sami, L., Boutaleb, A., Kolli, O., Haddouche, O., Demir, Y., Zedef, V., 2022. Evolution and genesis of fluorite mineralization in the Ouenza region (North-east of Algeria): Evidence from fluid inclusions and stable isotopes (C, O, and S). *Arab. J. Geosci.* 15 (6), 514. <https://doi.org/10.1007/s12517-022-09726-8>.
- Barbero, L., Teixell, A., Arboleya, M.-L., del Rio, P., Reiners, P.W., Bougadir, B., 2007. Jurassic-to-present thermal history of the central High Atlas (Morocco) assessed by low-temperature thermochronology. *Terra Nova* 19 (1), 58–64. <https://doi.org/10.1111/j.1365-3121.2006.00715.x>.
- Beauchamp, W., Barazangi, M., Demnati, A., ElAlji, M., 1996. Intracontinental rifting and inversion: Missour basin and Atlas Mountains, Morocco. *AAPG Bull. Am. Assoc. Pet. Geol.* 80 (9), 1459–1482.
- Beauchamp, J., 1988. Triassic sedimentation and rifting in the High Atlas (Morocco). In: Manspeizer, W. (Ed.), Triassic–Jurassic Rifting. In: Developments in Geotectonics, 22, 477–497. 10.1016/B978-0-444-42903-2.50025-7.
- Bill, H., 1982. Origin of the coloration of yellow fluorites: The O₃ center structure and dynamical aspects. *J. Chem. Phys.* 76 (1), 219–224. <https://doi.org/10.1063/1.442761>.
- Bill, H., Calas, G., 1978. Color centers, associated rare-earth ions and the origin of coloration in natural fluorites. *Phys. Chem. Miner.* 3 (2), 117–131. <https://doi.org/10.1007/BF00308116>.
- Boiron, M.C., Cathelineau, M., Banks, D.A., Buschaert, S., Fourcade, S., Coulibaly, Y., Michelot, J.L., Boyce, A., 2002. Fluid transfers at a basement/cover interface: Part II. Large-scale introduction of chlorine into the basement by Mesozoic basinal brines. *Chem. Geol.* 192 (1), 121–140. [https://doi.org/10.1016/S0009-2541\(02\)00191-2](https://doi.org/10.1016/S0009-2541(02)00191-2).
- Boiron, M.-C., Cathelineau, M., Richard, A., 2010. Fluid flows and metal deposition near basement /cover unconformity: Lessons and analogies from Pb-Zn-F-Ba systems for the understanding of Proterozoic U deposits. *Geofluids* 10 (1–2), 270–292. <https://doi.org/10.1111/j.1468-8123.2010.00289.x>.
- Bouabdellah, M., Castorina, F., Bodnar, R.J., Banks, D., Jebrak, M., Prochaska, W., Lowry, D., Klugel, A., Hoernle, K., 2014. Petroleum Migration, Fluid Mixing, and Halokinetics as the Main Ore-Forming Processes at the Peridiapiric Jbel Tirremi Fluorite-Barite Hydrothermal Deposit Northeastern Morocco. *Econ. Geol.* 109 (5), 1223–1256. <https://doi.org/10.2113/econgeo.109.5.1223>.
- Bouabdellah, M., Banks, D., Klugel, A., 2010a. Comments on “A late Triassic 40Ar/39Ar age for the El Hammam high-REE fluorite deposit (Morocco): Mineralization related to the Central Atlantic Magmatic Province?” by Cheillette et al. (*Mineralium Deposita* 45:323–329, 2010). *Mineralium Deposita*, 45(7), 729–731. 10.1007/s00126-010-0288-5.
- Bouabdellah, M., Hoernle, K., Kchit, A., Duggen, S., Hauff, F., Klugel, A., Lowry, D., Beaudoin, G., 2010b. Petrogenesis of the Eocene Tamazert Continental Carbonatites (Central High Atlas, Morocco): Implications for a Common Source for the Tamazert and Canary and Cape Verde Island Carbonatites. *J. Petrol.* 51 (8), 1655–1686. <https://doi.org/10.1093/petrology/eqq033>.
- Bouabdi, A., Dupuy, C., Dostal, J., 1988. Geochemistry of Mesozoic alkaline lamprophyres and related rocks from the Tamazeght massif, High Atlas (Morocco). *Lithos* 22, 43–58.
- Braithwaite, R.S.W., Flowers, W.T., Haszeldine, R.N., Russell, M., 1973. The cause of the colour of Blue John and other purple fluorites. *Mineral. Mag.* 39 (304), 401–411. <https://doi.org/10.1180/minmag.1973.039.304.0303>.
- Bühn, B., Rankin, A.H., Schneider, J., Dulski, P., 2002. The nature of orthomagmatic, carbonatic fluids precipitating REE, Sr-rich fluorite: Fluid-inclusion evidence from the Okorusu fluorite deposit Namibia. *Chem. Geol.* 186 (1), 75–98. [https://doi.org/10.1016/S0009-2541\(01\)00421-1](https://doi.org/10.1016/S0009-2541(01)00421-1).
- Burisch, M., Walter, B.F., Markl, G., 2017. Silification of hydrothermal gangue minerals in Pb-Zn-Cu-fluorite-quartz-baryte veins. *Can. Mineral.* 55 (3), 501–514. <https://doi.org/10.3749/canmin.1700005>.
- Burkhard, M., Carigt, S., Helg, U., Robert-Charrue, C., Soulaimani, A., 2006. Tectonics of the anti-atlas of Morocco. *C. R. Geosci.* 338 (1–2), 11–24. <https://doi.org/10.1016/j.crc.2005.11.012>.
- Camprubí, A., González-Partida, E., Richard, A., Boiron, M.-C., González-Ruiz, L., Aguilar-Ramírez, C., Fuentes-Guzmán, E., González-Ruiz, D., Legouix, C., 2019. MVT-Like Fluorite Deposits and Oligocene Magmatic-Hydrothermal Fluorite–Be–U–Mo–P–V Overprints in Northern Coahuila, Mexico. *Minerals* 9 (1), 58. <https://doi.org/10.3390/min9010058>.
- Cheillette, A., Gasquet, D., Filali, F., Archibald, D.A., Nespolo, M., 2010. A late Triassic 40Ar/39Ar age for the El Hammam high-REE fluorite deposit (Morocco): mineralization related to the Central Atlantic Magmatic Province? *Miner. Deposita* 45 (4), 323–329. <https://doi.org/10.1007/s00126-010-0282-y>.
- Choubert, G., Faure-Muret, A., 1962. Evolution du domaine atlasique marocain depuis les temps paléozoïques. *Mém. h. sér. Soc. géol. Fr. I.* 447–527.
- Chraibi, I., Talbi, F., Bouya, N., El Ouardi, H., 2013. REE geochemistry applied to the genetic study of fluorite in the mining district of El Hammam (Central Morocco). *Sociedad Geológica Española, Geogaceta* 54, 59–62. <http://hdl.handle.net/10272/7822>.
- Coşanay, P., Kirat, E., Çevik, N., Kızılkamat, C., Mutlu, H., Koç, Ş., 2017. Geochemical, microthermometric, and isotopic constraints on the origin of fluorite deposits in central Anatolia, Turkey. *Turk. J. Earth Sci.* 26, 206–226.
- Darimont, A., Coipel, J., 1982. Dispersion des températures d'homogénéisation des inclusions aqueuses — Ebullition ou division par étranglement. *Chem. Geol.* 37, 151–163. [https://doi.org/10.1016/0009-2541\(82\)90074-2](https://doi.org/10.1016/0009-2541(82)90074-2).
- Dill, H.G., Weber, B., 2010. Accessory minerals of fluorite and their implication regarding the environment of formation (Nabberg–Wölsendorf fluorite district, SE Germany), with special reference to fetid fluorite (“Stinkspat”). *Ore Geol. Rev.* 37 (2), 65–86. <https://doi.org/10.1016/j.oregeorev.2010.01.004>.
- Du Dresnay, R., 1971. Extention et développement des phénomènes récifaux Jurassiques dans le domaine atlasique marocain, particulièrement au Lias moyen. *Bull. Soc. Géol. France* 13 (7), 46–56.
- Du Dresnay, R., 1975. Influence de l'héritage structural tardi-hercynien et de la tectonique contemporaine de la sédimentation jurassique dans le sillon marin du Haut-Atlas, Maroc. Actes IXème Congrès International de Sédimentologie, Nice, thème 4: tectonique et sédimentation, 1, 103–108.
- Duan, Z.-P., Jiang, S.-Y., Su, H.-M., Zhu, X.-Y., Zou, T., Cheng, X.-Y., 2020. Trace and Rare Earth Elements, and Sr Isotopic Compositions of Fluorite from the Shihuiyao Rare Metal Deposit, Inner Mongolia: Implication for Its Origin. *Minerals* 10 (10), 882. <https://doi.org/10.3390/min10100882>.
- Ennih, N., Liegeois, J.P., 2001. The Moroccan Anti-Atlas: The West African craton passive margin with limited Pan-African activity. Implications for the northern limit of the craton. *Precambr. Res.* 112 (3–4), 289–302. [https://doi.org/10.1016/S0301-9268\(01\)00195-4](https://doi.org/10.1016/S0301-9268(01)00195-4).
- Fedan, B., Laville, E., El Mezqueldi, A., 1989. Le bassin Jurassique du Moyen-Atlas (Maroc): exemple de bassin sur relais de décrochements. *Bull. Soc. Géol. France*, série 8, 6, 1123–1136.
- Frizon de Lamotte, D., Saint Bezar, B., Bracène, R., Mercier, E., 2000. The two main steps of the Atlas building and geodynamics of the western Mediterranean. *Tectonics* 19 (4), 740–761. <https://doi.org/10.1029/2000TC900003>.
- Frizon de Lamotte, D., Leturmy, P., Misserand, Y., Khomsí, S., Ruiz, G., Saddiqi, O., Guillocheau, F., Michard, A., 2009. Mesozoic and Cenozoic vertical movements in the Atlas system (Algeria, Morocco, Tunisia): An overview. *Tectonophysics* 475 (1), 9–28. <https://doi.org/10.1016/j.tecto.2008.10.024>.
- Gaft, M., Waychunas, G.A., Rossman, G.R., Nagli, L., Panczer, G., Cheskis, D., Raichlin, Y., 2020. Red photoluminescence and purple color of naturally irradiated fluorite. *Phys. Chem. Miner.* 47 (11), 46. <https://doi.org/10.1007/s00269-020-01116-4>.
- Gagnon, J.E., Samson, I.M., Fryer, B.J., Williams-Jones, A.E., 2003. Compositional heterogeneity in fluorite and the genesis of fluorite deposits: insights from LA-ICP-MS analysis. *Can. Mineral.* 41 (2), 365–382. <https://doi.org/10.2113/gscmin.41.2.365>.
- Galwey, A.K., Jones, K.A., Reed, R., Dollimore, D., 1979. The blue coloration in banded fluorite (Blue John) from Castleton, Derbyshire, England. *Mineralogical Magazine* 43 (326), 243–250. <https://doi.org/10.1180/minmag.1979.043.326.06>.
- Gasquet, D., Ennih, N., Liegeois, J.-P., Soulaïmani, A., Michard, A., 2008. The Pan-African belt. In A. Michard, O. Saddiqi, A. Chalouan, D. F. D. Lamotte (Eds.), *Continental evolution: The geology of Morocco: Structure, stratigraphy, and tectonics of the Africa-Atlantic- Mediterranean triple junction*. Berlin, Heidelberg: Springer Berlin Heidelberg, pp. 33–64.
- Gigoux, M., 2015. Origine des minéralisations stratiformes de fluorine de la bordure sud-est du bassin de Paris. *Université Paris-Sud, p. 307 p. [Thèse de doctorat]*.
- Gigoux, M., Delpech, G., Guerrot, C., Pagel, M., Augé, T., Négrel, P., Brigaud, B., 2015. Evidence for an early Cretaceous mineralizing event above the basement/sediment unconformity in the intracratonic Paris Basin: Paragenetic sequence and Sm-Nd dating of the world-class Pierre-Perthuis stratabound fluorite deposit. *Miner. Deposita* 50 (4), 455–463. <https://doi.org/10.1007/s00126-015-0592-1>.
- Gigoux, M., Brigaud, B., Delpech, G., Guerrot, C., Augé, T., Négrel, P., 2016. Genetic constraints on world-class carbonate- and siliciclastic-hosted stratabound fluorite deposits in Burgundy (France) inferred from mineral paragenetic sequence and fluid inclusion studies. *Ore Geol. Rev.* 72, 940–962. <https://doi.org/10.1016/j.oregeorev.2015.09.013>.
- Goebel, L., 1930. Radioaktive Umwandlungerscheinungen am Fluorit von Wölsendorf. *Sitzungsberichte der Akademie der Wissenschaften mathematisch-naturwissenschaftliche Klasse, Abteilung I* 139, 373–391.
- Goldstein, R.H., Reynolds, T.J., 1994. Systematics of Fluid Inclusions in Diagenetic Minerals. *SEPM Society for Sedimentary Geology*. <https://doi.org/10.2110/scn.94.31>.
- González-Partida, E., Carrillo-Chávez, A., Grimmer, J.O.W., Pironon, J., Mutterer, J., Levresse, G., 2003. Fluorite deposits at Encantada-Buenavista, Mexico: Products of Mississippi Valley type processes. *Ore Geol. Rev.* 23 (3), 107–124. [https://doi.org/10.1016/S0169-1368\(03\)00018-0](https://doi.org/10.1016/S0169-1368(03)00018-0).

- Gu, H., Ma, D., Chen, W., Zhu, R., Li, Y., Li, Y., 2011. Electrolytic coloration and spectral properties of natural fluorite crystals containing oxygen impurities. *Spectrochim. Acta A Mol. Biomol. Spectrosc.* 82 (1), 327–331. <https://doi.org/10.1016/j.saa.2011.07.056>.
- Heitzmann, P., 1987. Le Trias dans le Haut Atlas central de Midelt Imilchil (Maroc): lithostratigraphic et signification tectonique. *Geologisches Institut der Universität Bern, Baltzerstrasse 1, CH 3012 Bern. Eclogae Geol. Helv.* 80 (3), 669–684.
- Jébrak, M., Debbah, B., Touray, J.-C., 1984. Saumures associées aux fluorines filonnierennes du Maroc Central, dans le district d'El Hammam. *Bull. Minér.* 107 (2), 233–240. <https://doi.org/10.3406/bulmi.1984.7755>.
- Jemmal, N., Carranza, E.J.M., Zemmel, B., 2017. Isotope geochemistry of Mississippi Valley Type stratabound F-Ba-(Pb-Zn) ores of Hammam Zriba (Province of Zaghouan, NE Tunisia). *Geochemistry* 77 (3), 477–486. <https://doi.org/10.1016/j.chemer.2017.07.003>.
- Jochum, K.P., Scholz, D., Stoll, B., Weis, U., Wilson, S.A., Yang, Q., Schwab, A., Börner, N., Jacob, D.E., Andreae, M.O., 2012. Accurate trace element analysis of speleothems and biogenic calcium carbonates by LA-ICP-MS. *Chem. Geol.* 318–319, 31–44. <https://doi.org/10.1016/j.chemgeo.2012.05.009>.
- Kchit, A., 2007. Pétrogenèse des carbonatites du complexe Alcalin de Tamazeght (Haut Atlas de Midelt, Maroc): contraintes imposées par les données des isotopes stables et radiogéniques. Université Mohamed Premier, Faculté des Sciences, Oujda, Doctorat d'Etat, p. 146p.
- Kchit, A., 1990. Le complexe plutonique alcalin du Tamazert, Haut Atlas de Midelt (Maroc). Pétrologie et structurologie. PhDthesis, Université de Toulouse, 302 p.
- Kempe, U., Plötz, M., Brachmann, A., Böttcher, R., 2002. Stabilisation of divalent rare earth elements in natural Fluorite. *Mineral. Petrol.* 76 (3), 213–234. <https://doi.org/10.1007/s007100200042>.
- Klitgord, K.D., Schouten, H., 1986. Plate kinematics of the central Atlantic. In: Vogt, P.R., Tucholke, B.E. (Eds.), *The Geology of North America, Volume M, The Western North Atlantic Region*. Geological Society of America, Denver, CO, pp. 351–378.
- Kynicky, J., Smith, M.P., Song, W., Chakhmouradian, A.R., Xu, C., Kopriva, A., Galiova, M.V., Brtnicky, M., 2019. The role of carbonate-fluoride melt immiscibility in shallow REE deposit evolution. *Geosci. Front.* 10 (2), 527–537. <https://doi.org/10.1016/j.gsf.2018.02.005>.
- Lanari, R., Fellin, M. G., Faccenna, C., Balestrieri, M. L., Pazzaglia, F. J., Youbi, N., Maden, C., 2020. Exhumation and Surface Evolution of the Western High Atlas and Surrounding Regions as Constrained by Low-Temperature Thermochronology. *Tectonics*, 39(3), e2019TC005562. 10.1029/2019TC005562.
- Laville, E., 1977. L'évolution sédimentaire et tectonique de la couverture jurassique de la région d'Immouzzer de Marmoucha (Moyen Atlas-Maroc). *Bulletin de la Société Géologique de France S7-XIX(5)*, 1151–1158. <https://doi.org/10.2113/gssgbull.S7-XIX.5.1151>.
- Laville, E., 1978. Incidence des jeux successifs d'un accident synsedimentaire sur les structures plicatives du versant nord du Haut Atlas central (Maroc). *Bulletin de la Société Géologique de France S7-XX(3)*, 329–337. <https://doi.org/10.2113/gssgbull.S7-XX.3.329>.
- Laville, E., 1985. Evolution sédimentaire, tectonique et magmatique du bassin Jurassique du Haut Atlas, Maroc: Modèle en relais multiples de décrochements. Thèse d'Etat, Montpellier, p. 168.
- Laville, E., Fedan, B., 1989. Le système atlasique marocain au jurassique. Evolution structurelle et cadre géodynamique. *Sci. Géol. Mém Strasbourg* 84, 3–28.
- Laville, E., Piqué, A., 1992. Jurassic penetrative deformation and Cenozoic uplift in the central High-Atlas (Morocco): a tectonic model. *Struct. Orogenic Inversions. Geol Rundsch* 81, 157–170. <https://doi.org/10.1007/BF01764546>.
- Laville, E., Lesage, J.-L., Seguret, M., 1977. Géométrie, cinématique (dynamique) de la tectonique atlasique sur le versant sud du Haut Atlas marocain; aperçu sur les tectoniques hercyniennes et tardi-hercyniennes. *Bulletin de la Société Géologique de France S7-XIX(3)*, 527–539. <https://doi.org/10.2113/gssgbull.S7-XIX.3.527>.
- Laville, E., Petit, J.-P., 1984. Role of synsedimentary strike-slip faults in the formation of Moroccan Triassic basins. *Geology* 12 (7), 424–427. [https://doi.org/10.1130/0091-7613\(1984\)12<424:ROSSPI>2.0.CO;2](https://doi.org/10.1130/0091-7613(1984)12<424:ROSSPI>2.0.CO;2).
- Laville, E., Piqué, A., 1991. La distension crustale atlantique et atlasique au Maroc au début du Mésozoïque: le rejeu des structures hercyniennes. *Bull. Soc. Géol. France* 162, 1161–1171.
- Laville, E., 1981. Rôle des décrochements dans le mécanisme de formation des bassins d'effondrement du Haut Atlas marocain au cours des temps triasique et liasique. *Bull. Soc. Géol. France*, (7), t. XXII, n° 1, pp. 303–312.
- Le Roy, P., Pique, A., Le Gall, B., Ait Brahim, L., Morabet, A.M., Demnati, A., 1997. Les bassins cotiers triasico-liasiques du Maroc occidental et la diachronie du rifting intra-continental de l'Atlantique central. *Bulletin de la Société Géologique de France* 168 (5), 637–648.
- Lenoir, L., Blaise, T., Somogyi, A., Brigaud, B., Barbarand, J., Boukari, C., Nouet, J., Brézard-Oudot, A., Pagel, M., 2021. Uranium incorporation in fluorite and exploration of U-Pb dating. *Geochronology* 3 (1), 199–227. <https://doi.org/10.5194/gchron-3-199-2021>.
- Leprétre, R., Missenard, Y., Saint-Bezar, B., Barbarand, J., Delpech, G., Yans, J., Dekoninck, A., Saddiqi, O., 2015. The three main steps of the Marrakech High Atlas building in Morocco: Structural evidences from the southern foreland, Imini area. *J. Afr. Earth Sc.* 109, 177–194. <https://doi.org/10.1016/j.jafrearsci.2015.05.013>.
- Liu, J., Zheng, M., Cook, N.J., Long, X., Deng, J., Zhai, Y., 2007. Geological and geochemical characteristics of the Sawaya'erdu gold deposit, southwestern Chinese Tianshan. *Ore Geol. Rev.* 32 (1-2), 125–156.
- Mackenzie, K.J.D., Green, J.M., 1971. The cause of coloration in Derbyshire Blue John banded fluorite and other blue banded fluorites. *Mineral. Mag.* 38 (296), 459–470. <https://doi.org/10.1180/minmag.1971.038.296.08>.
- Margoum, D., Bouabdellah, M., Klügel, A., Banks, D.A., Castorina, F., Cuney, M., Jébrak, M., Bozkaya, G., 2015. Pangea rifting and onward pre-Central Atlantic opening as the main ore-forming processes for the genesis of the Aouli REE-rich fluorite-barite vein system, Upper Moulaya District, Morocco. *J. Afr. Earth Sc.* 108, 22–39. <https://doi.org/10.1016/j.jafrearsci.2015.03.021>.
- Marks, M.A.W., Schilling, J., Coulson, I.M., Wenzel, T., Markl, G., 2008. The Alkaline-Peralkaline Tamazeght Complex, High Atlas Mountains, Morocco: Mineral Chemistry and Petrological Constraints for Derivation from a Compositionally Heterogeneous Mantle Source. *J. Petrol.* 49 (6), 1097–1131. <https://doi.org/10.1093/petrology/egn019>.
- Mattauer, M., Tappognier, P., Proust, F., 1977. Sur les mécanismes de formation des chaînes intracontinentales. L'exemple des chaînes atlasiques du Maroc. *Bulletin Société géologique France* 7 (XI), 521–526.
- Möller, P., Bau, M., Dulski, P., Lüders, V., 1998. REE and yttrium fractionation in fluorite and their bearing on fluorite formation. In Proceedings of the Ninth Quadrennial IAGOD Symposium; Hagni, R.D., Ed.; Schweizerbart: Stuttgart, Germany; pp. 575–592.
- Möller, P., Moretani, G., 1983. On the geochemical fractionation of rare earth elements during the formation of Ca-minerals and its application to problems of the genesis of ore deposits. In: Augustithis, S.S. (Ed.), *The Significance of Trace Elements in Solving Petrogenetic Problems and Controversies*. Theophrastus Pub, Athens, pp. 747–791.
- Möller, P., Parekh, P.P., Schneider, H.J., 1976. The application of Tb/Ca–Tb/La abundance ratios to problems of flourspar genesis. *Miner. Depos.* 11, 111–116.
- Möller, P., 1983. Lanthanoids as a geochemical probe and problems in lanthanoid geochemistry. Distribution and behavior of lanthanoids in non-magnetic-phases. In: Sinha, S.P. (ed.) *Systematics and the properties of the Lanthanides*; NATO-ASI, Ser. C, t. 109, p. 561–616.
- Olivet J.L., Bonnin J, Beuzart Paul, Auzende, J.M., 1984. Cinématique de l'Atlantique Nord et Central. Publications du Centre National pour l'Exploitation des Océans (CNEXO), Série Rapports scientifiques et techniques, n° 54, 1984 ISSN 0339-2899. <https://archimer.ifremer.fr/doc/00000/7439/>.
- Öztürk, H., Altuncu, S., Hanılıç, N., Kasapçı, C., Goodenough, K.M., 2019. Rare earth element-bearing fluorite deposits of Turkey: An overview. *Ore Geol. Rev.* 105, 423–444. <https://doi.org/10.1016/j.oregeorev.2018.12.021>.
- Palmer, D.A.S., Williams-Jones, A.E., 1996. Genesis of the carbonatite-hosted fluorite deposit at Amba Dongar, India; evidence from fluid inclusions, stability isotopes, and whole rock-mineral geochemistry. *Econ. Geol.* 91 (5), 934–950. <https://doi.org/10.2113/gseconeo.91.5.934>.
- Paton, C., Hellstrom, J., Paul, B., Woodhead, J., Hergt, J., 2011. Iolite: Freeware for the visualisation and processing of mass spectrometric data. *J. Anal. At. Spectrom.* 26 (12), 2508. <https://doi.org/10.1039/cjja10172b>.
- Pearce, N.J.G., Perkins, W.T., Westgate, J.A., Gorton, M.P., Jackson, S.E., Neal, C.R., Chenery, S.P., 1997. A Compilation of New and Published Major and Trace Element Data for NIST SRM 610 and NIST SRM 612 Glass Reference Materials. *Geostand. Geoanal. Res.* 21 (1), 115–144. <https://doi.org/10.1111/j.1751-908X.1997.tb00538.x>.
- Pei, Q., Zhang, S., Santosh, M., Cao, H., Zhang, W., Hu, X., Wang, L., 2017. Geochronology, geochemistry, fluid inclusion and C, O and Hf isotope compositions of the Shuitou fluorite deposit, Inner Mongolia, China. *Ore Geol. Rev.* 83, 174–190. <https://doi.org/10.1016/j.oregeorev.2016.12.022>.
- Piqué, A., Michard, A., 1989. Moroccan Hercynides—A synopsis—The Paleozoic sedimentary and tectonic evolution at the northern margin of West-Africa. *Am. J. Sci.* 289 (3), 286–330. <https://doi.org/10.2475/ajs.289.3.286>.
- Prokopyev, I., Kozlov, E., Fomina, E., Doroshkevich, A., Dyomkin, M., 2020. Mineralogy and Fluid Regime of Formation of the REE-Late-Stage Hydrothermal Mineralization of Petyayan-Vara Carbonatites (Vuoriyarvi, Kola Region, NW Russia). *Minerals* 10 (5), 405. <https://doi.org/10.3390/min10050405>.
- Putnis, A., 2009. Mineral Replacement Reactions. *Rev. Mineral. Geochem.* 70 (1), 87–124.
- Rajabzadeh, M.A., 2007. A fluid inclusion study of a large MVT barite–fluorite deposit: Komshcheh, Central Iran. *Iranian J. Sci. Tech.* 31, 73–87.
- Ramamohana Rao, N.V., Rao, N., Surya Prakash Rao, K., Schuiling, R. D., 1993. Fluorine distribution in waters of Nalgonda District, Andhra Pradesh, India. *Geo* 21, 84–89. 10.1007/BF00775055.
- Rankin, A.H., Ni, P., Zhou, J., 2003. Fluid inclusion studies on carbonatite dyke and associated quartzite in Bayan Obo, Inner Mongolia China. *Acta Petrologica Sinica* 19 (2), 297–306.
- Redina, A.A., Nikolenko, A.M., Doroshkevich, A.G., Prokopyev, I.R., Wohlgemuth-Ueberwasser, C., Vladykin, N.V., 2020. Conditions for the crystallization of fluorite in the Mughai-Khudag complex (Southern Mongolia): Evidence from trace element geochemistry and fluid inclusions. *Geochemistry* 80 (4), 125666. <https://doi.org/10.1016/j.chemer.2020.125666>.
- Redina, A.A., Doroshkevich, A.G., Veksler, I.V., Wohlgemuth-Ueberwasser, C.C., 2021. Fluorite Mineralization Related to Carbonatite Magmatism in the Western Transbaikalia: Insights from Fluid Inclusions and Trace Element Composition. *Minerals* 11 (11), 1183. <https://doi.org/10.3390/min11111183>.
- Ricou, L.E., 1994. Tethys reconstructed: Plates, continental fragments and their boundaries since 260 Ma from Central America to South-eastern Asia. *Geodin. Acta* 7 (4), 169–218.
- Roedder, E., 1979. Fluid inclusions as samples of ore fluids. In: Barnes, H.L. (Ed.), *Geochemistry of Hydrothermal Ore Deposits*, second ed. Wiley-Interscience, New York, pp. 684–737.
- Roedder, E., 1984. Fluid inclusions: An introduction to studies of all types of fluid inclusions, gas, liquid, or melt, trapped in materials from earth and space, and their application to the understanding of geologic processes. *Mineralogical Society of America*.

- Salvi, S., Fontan, F., Monchoux, P., Williams-Jones, A.E., Moine, B., 2000. Hydrothermal Mobilization of High Field Strength Elements in Alkaline Igneous Systems: Evidence from the Tamazeght Complex (Morocco). *Econ. Geol.* 95 (3), 559–576. <https://doi.org/10.2113/gsecongeo.95.3.559>.
- Sánchez, V., Vindel, E., Martín-Crespo, T., Corbella, M., Cardellach, E., Banks, D., 2009. Sources and composition of fluids associated with fluorite deposits of Asturias (N Spain). *Geofluids* 9 (4), 338–355. <https://doi.org/10.1111/j.1468-8123.2009.00259.x>.
- Sar, S., Samuelsson, C., Engström, F., Ökvist, L.S., 2020. Experimental study on the dissolution behavior of calcium fluoride. *Metals* 10 (8), 1–12. <https://doi.org/10.3390/met10080988>.
- Schilling, J., Marks, M.A.W., Wenzel, T., Markl, G., 2009. Reconstruction of magmatic to subsolidus processes in an aplitic system using eudialyte textures and composition: A case study from Tamazeght, Morocco. *Canadian Mineralogist* 47 (2), 351–365. <https://doi.org/10.3749/canmin.47.2.351>.
- Schönenberger, J., Köhler, J., Markl, G., 2008. REE systematics of fluorides, calcite and siderite in peralkaline plutonic rocks from the Gardar Province, South Greenland. *Chem. Geol.* 247 (1), 16–35. <https://doi.org/10.1016/j.chemgeo.2007.10.002>.
- Sheard, E.R., Williams-Jones, A.E., Heiligmann, M., Pederson, C., Trueman, D.L., 2012. Controls on the Concentration of Zirconium, Niobium, and the Rare Earth Elements in the Thor Lake Rare Metal Deposit, Northwest Territories Canada. *Econ. Geol.* 107 (1), 81–104. <https://doi.org/10.2113/econgeo.107.1.81>.
- Simonetti, A., Bell, K.F., 1995. Nd, Pb, and Sr isotope systematics of fluorite at the Amba Dongar carbonatite complex, India; evidence for hydrothermal and crustal fluid mixing. *Econ. Geol.* 90, 2018–2027.
- Singh, T., Upadhyay, D., Patel, A.K., Mishra, B., 2022. High MREE-HREE solubility in a carbonatite-derived hydrothermal fluid: Evidence from fluorite-hosted fluid inclusions in the Amba Dongar carbonatite complex India. *Chem. Geol.* 613, 121162. <https://doi.org/10.1016/j.chemgeo.2022.121162>.
- Sizaret, S., Marcoux, E., Jébrak, M., Touray, J.C., 2004. The Rossignol Fluorite Vein, Chaillac, France: Multiphase Hydrothermal Activity and Intravein Sedimentation. *Econ. Geol.* 99 (6), 1107–1122. <https://doi.org/10.2113/gsecongeo.99.6.1107>.
- Sizaret, S., Marcoux, E., Boyce, A., Jébrak, M., Stevenson, R., Ellam, R., 2009. Isotopic (S, Sr, Sm/Nd, D, Pb) evidences for multiple sources in the Early Jurassic Chaillac F-Ba ore deposit (Indre, France). *Bulletin de La Société Géologique de France* 180 (2), 83–94. <https://doi.org/10.2113/gssgbull.180.2.83>.
- Smith, M.P., Campbell, L.S., Kynicky, J., 2015. A review of the genesis of the world class Bayan Obo Fe-REE-Nb deposits, Inner Mongolia, China: Multistage processes and outstanding questions. *Ore Geol. Rev.* 64, 459–476. <https://doi.org/10.1016/j.oregeorev.2014.03.007>.
- Sošnicka, M., Rddad, L., Kraemer, D., 2021. Preliminary fluid inclusion study of fluorite deposits adjacent to the Tamazert alkaline igneous complex, Morocco. In: The 26th edition European current research on fluid and melt inclusions (International congress e-CROFI), p. 33.
- Steele-MacInnis, M., Lecumberri-Sánchez, P., Bodnar, R.J., 2012. Short note: HokieFlincs_H2O-NaCl: a Microsoft Excel spreadsheet for interpreting microthermometric data from fluid inclusions based on the PVTX properties of H2O-NaCl. *Comput. Geosci.* 49, 334–337. <https://doi.org/10.1016/j.cageo.2012.01.022>.
- Stefánsson, A., Bénézeth, P., Schott, J., 2013. Carbonic acid ionization and the stability of sodium bicarbonate and carbonate ion pairs to 200°C - A potentiometric and spectrophotometric study. *Geochim. Cosmochim. Acta* 120, 600–611. <https://doi.org/10.1016/j.gca.2013.04.023>.
- Studer, M., Du Dresnay, R., 1980. Déformations synsédimentaires en compression pendant le Lias supérieur et le Dogger au Tizi n'Irlil (Haut Atlas central de Midelt Maroc). *Bull. Soc. géol. France* (7) 22 (3), 391–397.
- Sun, S.S., McDonough, W.F., 1989. Chemical and isotopic systematics of oceanic basalts: implications for mantle composition and processes. *SP* 42 (1), 313–345.
- Tapponnier, P., 1977. Evolution tectonique du système alpin en Méditerranée; poinconnement et érastement rigide-plastique. *Bulletin de la Société Géologique de France* S7-XIX(3), 437–460. <https://doi.org/10.2113/gssgbull.S7-XIX.3.437>.
- Thomas, R.J., Chevallier, L.P., Gresse, P.G., Harmer, R.E., Eglington, B.M., Armstrong, R. A., de Beer, C.H., Martini, J.E.J., de Kock, G.S., Macey, P.H., Ingram, B.A., 2002. Precambrian evolution of the Siwa Window, Anti-Atlas Orogen Morocco. *Precambr. Res.* 118 (1–2), 1–57. [https://doi.org/10.1016/S0301-9268\(02\)00075-X](https://doi.org/10.1016/S0301-9268(02)00075-X).
- Tisserant, D., R. Thuijat, Agard, J., 1976. Données géochronologiques sur le complexe de roches alcalines du Tamazeght (Haut Atlas de Midelt, Maroc). Bureau des recherches géologiques et minières bulletin, 2: p. 279–283. (Cf. p. 23).
- Van den Kerkhof, A.M., Hein, U.F., 2001. Fluid inclusion petrography. *Lithos* 55 (1–4), 27–47. [https://doi.org/10.1016/S0024-4937\(00\)00037-2](https://doi.org/10.1016/S0024-4937(00)00037-2).
- Van den Kerkhof, A. M., 1988. The system CO₂-CH₄-N₂ in fluid inclusions: theoretical modelling and geological applications.
- Vochten, R.F.C., Geys, J.F., 1977. Solid inclusions in a fluorite variety from the Wölsendorfer Range (Bavaria, Fed. Rep. Germany). *Schweiz. Mineral. Petrogr. Mitt.* 57, 23–30.
- Wang, L.-X., Marks, M.A.W., Wenzel, T., Markl, G., 2016. Halogen-Bearing Minerals from the Tamazeght Complex (Morocco): Constraints on Halogen Distribution and Evolution In Alkaline To Peralkaline Magmatic Systems. *Can. Mineral.* 54 (6), 1347–1368. <https://doi.org/10.3749/canmin.1600007>.
- Xu, C., Taylor, R.N., Li, W., Kynicky, J., Chakhmouradian, A.R., Song, W., 2012. Comparison of fluorite geochemistry from REE deposits in the Panxi region and Bayan Obo, China. *J. Asian Earth Sci.* 57, 76–89. <https://doi.org/10.1016/j.jseas.2012.06.007>.
- Ye, X., Bai, F., 2022. Spectral Characteristics, Rare Earth Elements, and Ore-Forming Fluid Constrains on the Origin of Fluorite Deposit in Nanlishu, Jilin Province, China. *Minerals* 12 (10), 1195. <https://doi.org/10.3390/min12101195>.
- Zheng, Y.F., 1999. Oxygen isotope fractionation in carbonate and sulfate minerals. *Geochem. J.* 33, 109–126. <https://doi.org/10.2343/geochemj.33.109>.